VALIDATION

POOL VAPORISATION

DATE: December 2023

No.	Date	Reason for Issue	Prepared by	Verified by	Approved by
1	Oct 2012	Moved validation from PVAP theory document; added experiments by Reijnhart & Rose, and Norman & Dowell	Maria Fernandez	Henk Witlox	
2	May 2021	Apply template	D. Vatier		
3	July 2022	Version update	David Worthington		

Date: December 2023

Prepared by: Digital Solutions at DNV

ABSTRACT

This report describes the validation for PVAP pool spreading and vaporisation model. The validation gives an account of the level of confidence of PVAP results for experiments carried out on land and water. The pool spreading and vaporisation PVAP models were validated both independently and coupled.

General good agreement with the experimental data was found for boiling on land and water models, spreading on land and simultaneous spreading and vaporisation on land. Evaporation on land and spreading on water models were found to give too conservative estimates.

The validation highlighted areas for improvement for the modelling of evaporating pools on land, the modelling of pool spreading on water, and the values given to the minimum thickness for pools on land.

Table of contents

Table of figures

List of tables

1 INTRODUCTION

The aim of this report is to present the results of a series of validation tests for the pool model PVAP, with the aim of providing a measure of the accuracy of the model against real data and highlighting possible areas of improvement.

Over the years, experimental data for the spreading and vaporisation of hazardous spills has been collected by different authors, e.g. Prince[1], Thyer[2] [3], Luketa-Hanlin[4]. In this work, reference is made to these reports as they provide a measure of the reliability of the experimental data. Other sources of experimental data for pool validation have also been consulted, Hanna[5], Webber et al.6.

The validation data set comprises a total of twelve sets of experiments, seven sets to validate the performance of pools on land surfaces and five on water surfaces.
Table 1 provides a summary of the validation experiments; a more detailed description is presented in Chapter 4 of this document. The validation data set includes the validation description originally included in the PVAP theory manual (as marked by * in
Table 1), and additional experiments (not marked by * in
Table 1).

The selection of the experiments was made on the basis of covering a wide range of conditions including: pure components and mixtures, with low and high volatilities, different surfaces (soil, concrete, water) in the presence of bunds or not, and from instantaneous and continuous releases.

The plan of this report is as follows: Chapter 2 provides information about method of PVAP model simulation of the experiments, including selection of input data and treatment of output results; Chapter 3 shows the model validation results obtained for the test runs; finally, Chapter 4 presents the list of future work, based on the conclusions extracted from this work.

Experiment	Number of runs	Surface	Indoors/ Outdoors	Spill	Substance(s) tested	Scale	Model validated
Belore and McBean*	3	Plywood	Indoors	Continuous	Water	Large	Spreading on land
Reid and Wang*	8	Soil/ Concrete	Indoors	Instantaneous	LNG	Small/ Medium	Boiling on land
Kawamura and MacKay*	6	Sand	Outdoors	Instantaneous	Hydrocarbons	Medium	Evaporation on land
Reijnhart and Rose	6	Insulated surface	Indoors	Instantaneous	Toluene/ Pentane	Small/ Medium	Evaporation on land
Norman and Dowell	7	Insulated surface	Outdoors	Instantaneous	Various refrigerants and other chemicals	Medium	Evaporation on land
Okamoto et al	3	Insulated surface	Indoors	Instantaneous	Binary and ternary mixtures of hydrocarbons	Small	Evaporation on land
Habid et al	2	Insulated surface	Outdoors	Instantaneous	Ethanol / Cyclohexane	Medium	Evaporation on land
Moorhouse and Carpenter	2	Soil/ Concrete	Outdoors	Continuous	LNG	Very large	Simultaneous spreading and vaporisation on land
Dodge*	4	Water	Outdoors	Instantaneous/Continuous	N-Pentane/ N-Octane	Large	Spreading on water
Bureau of Mines	22	Water	Indoors	Instantaneous	LNG / Nitrogen	Medium	Boiling on water
Reid and Smith*	6	Water/Ice	Indoors	Instantaneous/Continuous	LPG/Ethane/ Ethylene/ N-Butane	Small/ Medium	Boiling on water
Burro Series	2	Water	Outdoors	Continuous	LNG	Very large	Simultaneous spreading and vaporisation on water
Raj and Reid*	12	Water	Indoors	Instantaneous/Continuous	Ammonia	Small/ Medium/Large	Reactive dissolution on water

Table 1. Summary of experiments used for validation

2 METHOD FOR PVAP SIMULATION OF EXPERIMENTS

2.1 Input data

A comprehensive list of input data applied for each of the validation experiments can be found in Appendix A. The input data for the simulations were obtained from the references listed at the end of the report. However, not all the model input data required for the PVAP simulations are reported in the references. Therefore, the following general assumptions have been made:

- Cryogenic chemicals are spilled as saturated liquids. This applies to the following experimental sets: Reid and Wang[vii], Moorhouse and Carpenter[viii], Bureau of Mines[ix], Reid and Smith[x], Burro Series[xi] and Raj and Reid[xii]. For the remaining experiments the air temperature is taken as the temperature of the spill, unless otherwise specified.

- Default surface PVAP properties are used, except in those cases were properties are specified by the reference or the surface does not correspond to a default surface in PVAP

- For experiments carried out indoors – Reid and Wang[vii]; Bureau of Mines[ix]; Reid and Smith[x]; Okamoto et al.[xiii]; Raj and Reid[xii]; and Belore and McBean[xiv] – the following default physical data were used as input when no experimental data was provided:

  - Pasquill stability class = F (stable)[1]
  - Solar radiation flux (W/m^2) = 0
  - Wind speed at reference height (m/s) = 0.1001
  - Reference height for wind speed measurement (m) = 10
  - Ambient temperature (K) = 293
  - Ambient pressure (Pa) = 101,325

- Outdoors experiments and wind tunnel experiments – Moorhouse and Carpenter[viii]; Kawamura and MacKay[xv]; Burro series[xi]; Norman and Dowell[xvi]; Reijnhart and Rose[xvii]; Habid et al.[xviii]; and Dodge, et al.[xix] – used the following as default physical parameters:

  - Pasquill stability class = D (neutral)
  - Solar radiation flux (W/m^2) = 500
  - Reference height for wind speed measurement (m) = 10
  - Ambient pressure (Pa) = 101,325

- As Kawamura and MacKay[xv] reported average evaporation rates determined for the total duration of each experiment, the cut-off rate of the vaporisation was set to a very low value (10^{-7} kg/s), to ensure the PVAP simulations won't stop before the total duration reported by the authors.

- For Reijnhart and Rose[xvii] series of experiments the wind speed was reported by the authors as the average of wind-speed across the turbulent boundary layer, presuming a logarithmic wind profile as a function of height. The following procedure shows how the wind speed at 1 m above the pool was calculated:

  a) Given the roughness length of the surface (z_0), average height of the logarithmic wind profile along the length of the pool (z_l) and the average wind speed in the logarithmic profile (u_{av}), choose the reference height for the wind speed (z) (10 m above the pool).

  b) From Reijnhart et al.[xx] model the average wind speed on the logarithmic profile above the pool is defined as:

$$u_{av} = \frac{u_1^*}{\kappa}\left[Ln\left(\frac{z_l}{z_1}\right) - 1\right] \quad \textbf{(1)}$$

where:

- κ is Von Karman's constant

[1] For such low wind speeds as the ones present in these indoors experiments selecting an stable (F) or neutral (D) stability class has insignificant impact on the pool results

- u_1^* is the friction velocity above the pool surface

- z_1 is the effective liquid pool surface roughness:

$$z_1 = \frac{\upsilon_m}{u_1^* 5.1\kappa} \quad \textbf{(2)}$$

- υ_m is the kinematic viscosity of air ($1.5 \cdot 10^{-5}$ m^2/s at 25 ^oC, 1 atm)

Substituting equation (2) into (1) the friction velocity u_1^* is obtained by an iterative solution. With the friction velocity, the wind velocity at a given reference height is calculated in the next step.

c) Reijnhart et al.[xx] considers the surface of the pool to be smooth, therefore the wind profile in the turbulent layer is given as:

$$u(z) = \frac{u_1^*}{\kappa} Ln\left(\frac{u_1^* z}{\upsilon_m}\right) + 5.1u_1^* \quad \textbf{(3)}$$

where: *u(z)* is the wind speed at the reference height (*z*)

- For Habid et al.[xviii] experiments the solar radiation flux was not measured for the duration of the tests. For the PVAP simulations, it was estimated from the formula in the Yellow Book[xxi]:

$$H_{rs} = (C_1 \sin \chi - C_2)(1 - 0.75N^{3.4}) \quad \textbf{(4)}$$

where,

- H_{rs} is the incoming solar radiation flux, in PVAP nomenclature this is *S* (W/m^2)

- C_1 is a constant = 990 (W/m^2)

- C_2 is a constant = 30 (W/m^2)

- χ is the solar elevation, which depends on the geographical position and time of the year

- *N* is the cloud cover

The solar elevation angle was determined from the database provided by the National Oceanic and Atmospheric Administration[xxii] of the US Department of Commerce, given the geographical coordinates of the test site (Berlin, Germany) and time of the year (summer). The results gave an average solar elevation of 52^o and 50^{o}for the time and date of the ethanol and cyclo-hexane experiments[2].

The cloud cover which Habid et al.[xviii] reported varied during the experiments was given a range of values from 20 to 50%.

- The validation against Reid and Wang[vii], Moorhouse and Carpenter[viii] and Norman and Dowell[xvi] experiments was done with MacKay and Matsugu[xxiii] evaporation on land equation. Validations against Kawamura and MacKay[xv] and Reijnhart and Rose[xvii] experiments report the results of the three equations for evaporation on land (Phast 6.7, MacKay and Matsugu[xxiii], Opschoor (1978)[xxiv]). The formulas for the evaporation on land can be found in the Appendix B.

2.2 Output data

2 Date and time of the experiments provided by private communication with Habid

PVAP generates arrays over time for predictions for the main experimentally measured data, i.e. the mass vaporised (kg), vaporisation rate (kg/s), pool radius (m) and temperature (K). For certain experimental datasets, these PVAP output data required additional post processing to enable a comparison with the reported measured data.

For experiments that reported the evaporation flux or mass vaporised per unit area, the simulated evaporation rate or mass vaporised was calculated per unit of area of the pool.

The Kawamura and MacKay[xv] set of experiments report the evaporation rate for each test as the average over the duration of the test. For PVAP simulations this averaged rate is determined as:

$$E_{vap\ ave} = \frac{\sum_{j=1}^{m} E_{vap}{}^{j} \Delta t_j}{t} \quad \textbf{(5)}$$

where,

$E_{vap\ ave}$	is the average evaporation rate (kg/s) over the duration of the experiment
$E_{vap}{}^{j}$	is the evaporation rate (kg/s) during the time interval Δt_j, taken as the average of the evaporation rate at the start and end of the time interval
Δt_j	is the time interval (s)
t	is the duration of the experiment (s)
j	is the index indicating the current time step
m	is the total number of time steps

Reijnhart and Rose[xvii] experiments report the data as the reduced evaporation rate $E_{vap\ reduced}$ given by:

$$E_{vap\ reduced} = \frac{E_{vap} \cdot R \cdot T_{pool}}{P_v^{\,c}(T_{pool}) \cdot M_c} \quad \textbf{(6)}$$

Where R = 8314 J/K/kmol is the gas constant, T_{pool} the pool temperature (K), M_c the molecular weight (kg/kmol) of the spilled liquid, and $p_v^c(T_{pool})$ the saturated vapour pressure (Pa) of the liquid.

3 MODEL VALIDATION RESULTS AND DISCUSSION

This section discusses the results obtained from the model validation for both pools on land and pools on water.

The validation is carried out in successive steps:

- Firstly, the pool spreading models were tested by comparison with experimental data for the spreading of chemicals with very low volatility.
- Secondly the vaporisation models for boiling and non-boiling evaporating pools are validated against experimental data for spills in confined areas where spreading does not take place.
- Lastly, comparisons are made for simultaneously spreading and vaporising pools.

The first above two steps essentially decouples the testing of the spread rate from testing the evaporation rate, while the third step tests spreading and evaporation simultaneously.

Additionally validation of the reactive dissolution model for ammonia pools on water is included.

3.1 Pools on land

3.1.1 Pool spreading

Belore and McBean[xiv] performed a series of experiments to observe pool spreading behaviour. The tests were carried out in a 3m x 3m bed. Water, a relatively non-volatile chemical, was used. Calculations were made with the model simulating the plywood surface as concrete.

Figure 1 shows for test 28 PVAP predictions for the pool radius r as function of time t for two values of minimum pool thickness, i.e. h_{min} = 0.005m and 0.01m[3]. While the simulated results obtained using either value of pool thickness is observed to fit experimental data reasonably well, the best fit to the experimental data is likely to lie in-between both values.

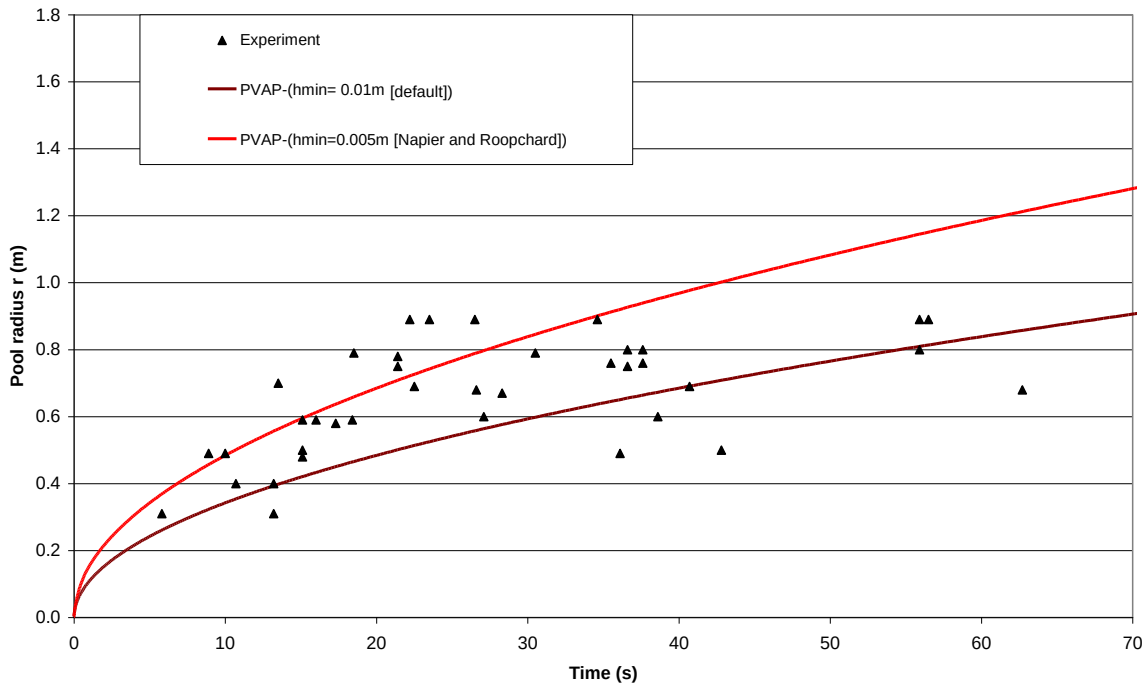

Figure 1 PVAP predictions for pool radius (continuous spill, water on plywood, Belore and McBean[xiv] test 28)

Figure 2 includes PVAP predictions for pool radius as function of time for tests 28-30 corresponding to different water spill rates on plywood and assuming a minimum pool thickness of 0.005m[4]. Figure 3 shows the predicted against experimental

[3] h_{min} = 0.01m represents the adopted minimum pool thickness for concrete in Phast 6.42 and earlier versions.

[4] h_{min} = 0.005 m is the adopted default minimum pool thickness for concrete

pool radius. In general it can be observed that the model over predicts the experimental pool radius, as most of the data points lay above the diagonal. The best fit to the experimental data is found at lower mass flows (run 28 – 0.367 kg/s).

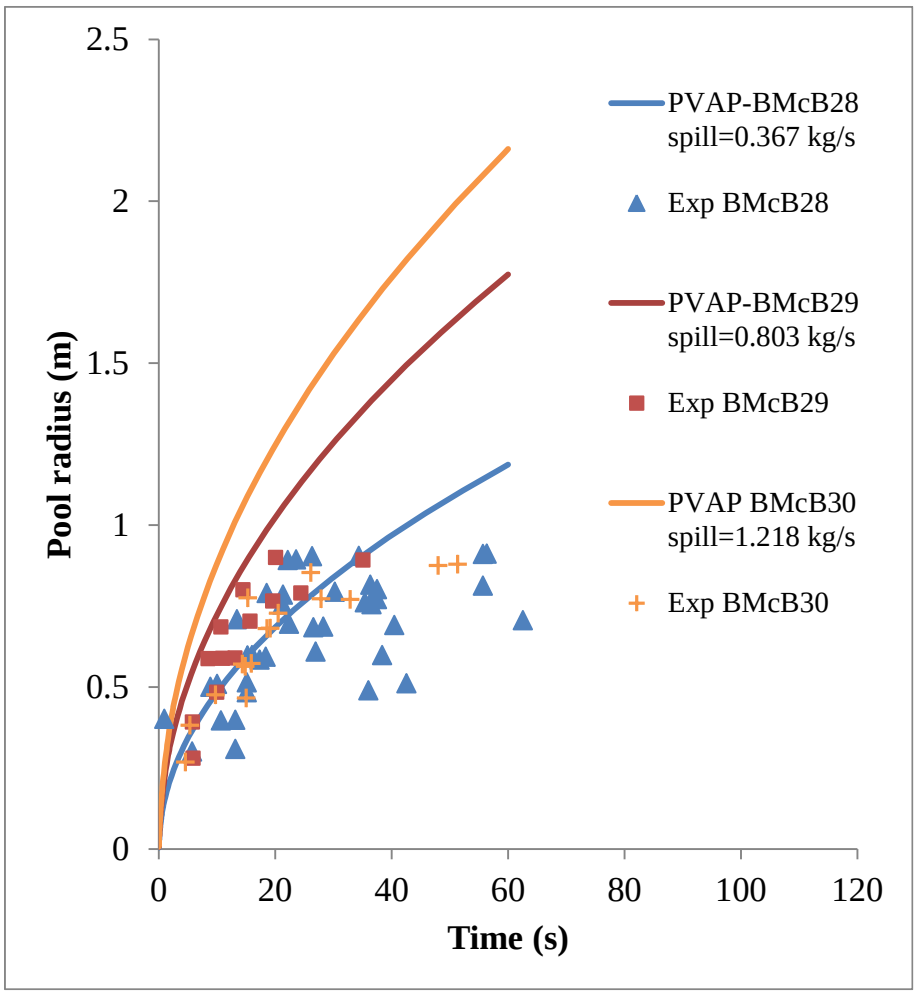

Figure 2 **Comparison of model calculation with experimental data Belore and McBean[xiv] for the spreading of water continuously spilt on plywood. Test numbers BMcB28 to BMcB30**

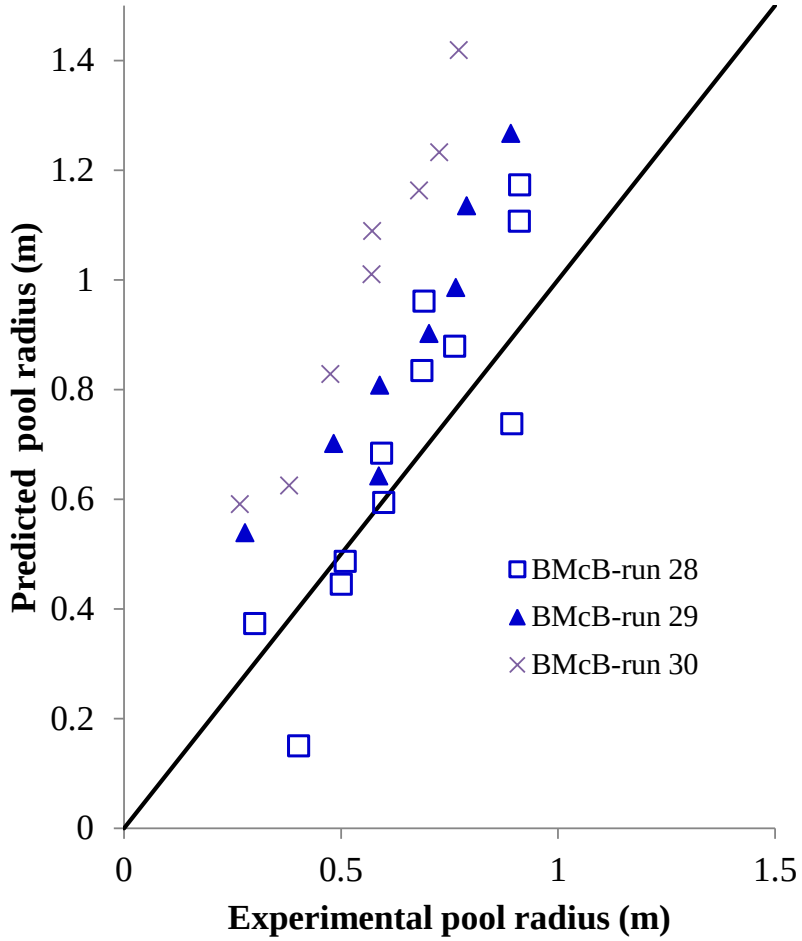

Figure 3 **Predicted against experimental Belore and McBean[xiv] pool radius for water on plywood h_{min} = 0.005m**

3.1.2 Pool vaporisation

Reid and Wang[vii] spilled LNG onto different dike floor materials, insulated concrete, wet soil, sand, polyurethane and corrugated aluminium. An insulating top cover was used to eliminate the contribution from the convective heat transfer between the LNG and air, and to ensure that the spilled fluid remained at the boiling regime. Surface temperature and pool weight measurements were made every second. Test runs made on concrete and soil were included in the validation set. Figure 4 shows the calculated and experimental mass vaporised as a function of $t^{1/2}$ for a spill of LNG on insulated concrete. It is seen that they agree very well.

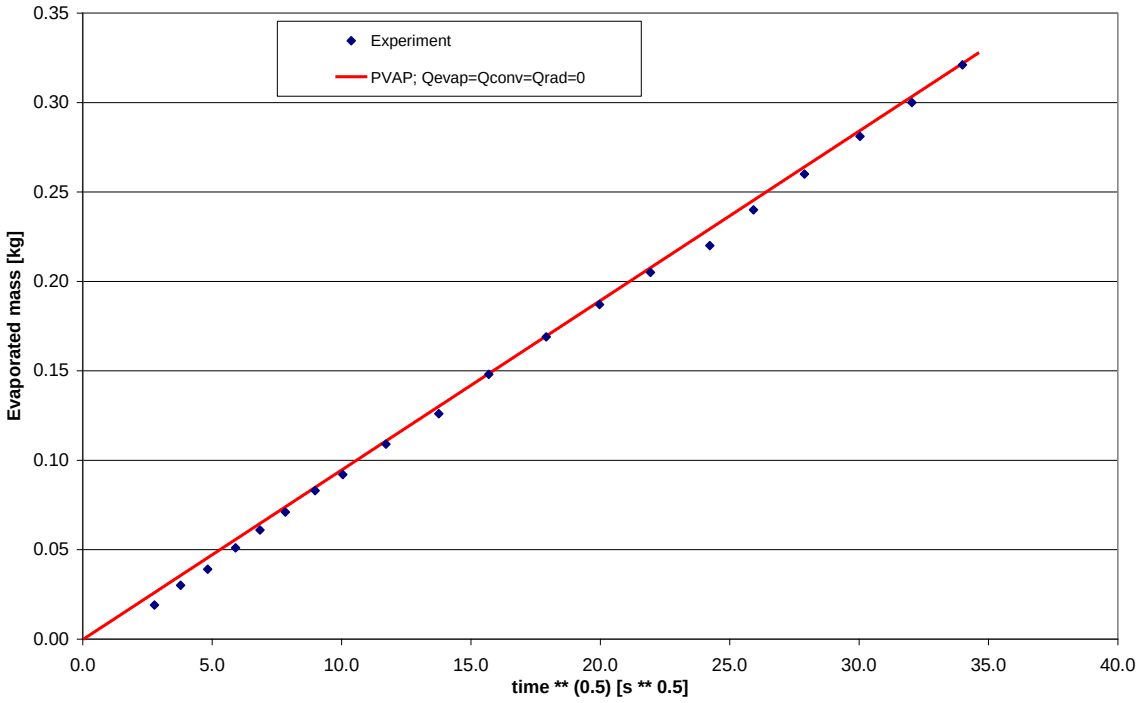

Figure 4 **Comparison of model calculation with experimental data Reid and Wang[vii] for the boiling of LNG on insulated concrete (test RW70)**

Figure 5 presents the predicted against experimental percentage of mass vaporised to total mass spilled for Reid and Wang[vii] experiments of LNG on soil and concrete. General good correspondence is observed between modelled and experimental data. Vaporisation of only +10% of the spilled mass for RW45 (in soil) is reported here as authors observed percolation of LNG into the soil at early stages of the spill. The properties of the soil used in this comparison correspond to the soil used in Reid and Wang[vii] experiments. The following table compares the soil properties reported by Reid and Wang[vii] and the ones stored in PVAP's database:

Reference	k_s (W/m K)	F (kg/m^2 s$^{0.5}$)
Reid and Wang (1978)	~6	0.5 (up to 8% water content in soil)
Gaz de France (1972)	---	1 (dry) - 1.5 (wet)
Drake and Reid (1975)	---	0.3-0.5
PVAP wet soil	2.2	1.1-1.2
PVAP dry soil	0.32	0.32-0.35

Table 2 **Comparison of the thermal properties of different soils reported by Reid and Wang[vii] and PVAP**

Where k_s is the thermal conductivity and F is given as: $$F = \frac{\chi_s \cdot k_s \cdot \left(T_{surf} - BPT\right)}{\pi^{0.5} \cdot \alpha_s^{\,0.5} \cdot \Delta H_{vap}}$$

T_{surf} is the initial temperature of the surface and BPT is the normal boiling point of the chemical, and the rest of the symbols are as defined in PVAP Theory Manual.

The parameter F can be obtained from the slope of the curve of the total mass vaporized against the square root of time for a boiling pool of constant radius (Reid and Wang[vii]).

PVAP soil properties have been taken from Gaz de France[xxv] and Drake and Reid[xxvi] studies on soils with different levels of humidity. The differences found in the values reported in the literature convey the difficulty of establishing standard properties for soil.

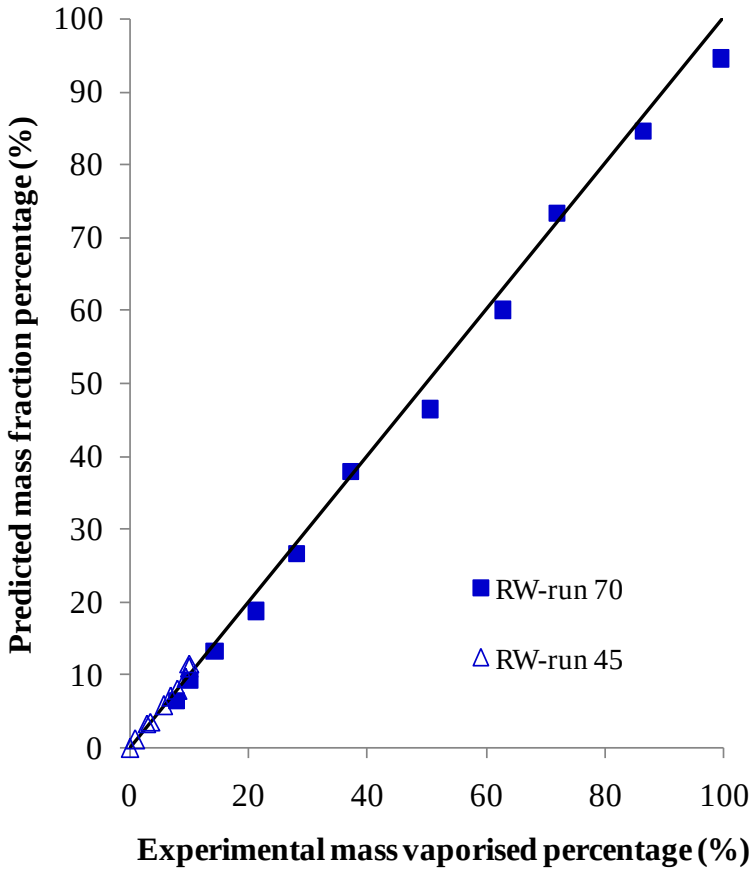

Figure 5 Predicted against experimental (Reid and Wang[vii]) percentage of mass vaporised on soil (RW45) and concrete (RW70)

Kawamura and MacKay[xv]: Two series of simple outdoor evaporation tests for a range of materials (toluene, hexane, pentane, cyclo-hexane and Freon 11) were carried out by Kawamura and MacKay[xv] on sand and over an insulated surface. The evaporation of the chemicals was measured by the depletion of a reservoir connected to an evaporating pan of inner diameter equal to 0.46 m. Average evaporation rates were determined for the duration of the tests. Test runs with insulation were not included as part of the validation set due to lack of wind speed data. Table 3 presents a comparison between the experimental and predicted data of averaged evaporation rates for four tests selected from Kawamura and MacKay[xv] on a sand surface. The table includes results for the three different evaporation models available for the Phast 7 standalone PVAP-MC model, i.e. the original PVAP formulation in Phast 6.7, the model by MacKay and Matsugu[xxiii], and the model by Opschoor[xxiv]; see Appendix B for the formulas adopted for the heat of evaporation by these three models.

Test number	KM18	KM20	KM21	KM22	KM19	KM23
Chemical	Toluene	Hexane	Pentane	Pentane	Cyclo-hexane	Freon11
Temperature of the spill	296.15	298.15	298.15	300.15	302	295
Wind speed at 10 m height (m/s)	2.65	1.59	4.94	5.42	3.14	1.17
Experimental evaporation rate ($kg/m^2.h$)	3.9	7.28	23	27.1	9.38	34.88
PVAP in Phast 6.7 evaporation rate ($kg/m^2.h$) Deviation PVAP in Phast 6.7 (%)	5.68 +45%	14.05 +92%	27.68 +20%	34.45 +27%	13.98 +49%	61.72 +77%
MacKay and Matsugu (1973) evaporation rate ($kg/m^2.h$) Deviation MacKay and Matsugu (1973) (%)	4.42 +13%	10.31 +42%	27.08 +18%	33.79 +25%	11.85 +26%	41.66 +19%
Opschoor (1979) evaporation rate ($kg/m^2.h$) Deviation Opschoor (1978) (%)	3.16 -19%	9.32 +28%	30.90 +34%	31.85 +18%	10.56 +13%	41.91 +20%

Table 3 Comparison of the average evaporation rates model calculations against experimental data (Kawamura and MacKay[xv]) on sand surface

From
Table 3 it is observed that the highest deviation between model and experimental data is obtained for the original Phast 6.7 model with a volatile substance (hexane). The best agreement between model data is given by MacKay and Matsugu[xxiii] equation at a low vapour pressure material (toluene). On the other hand, Opschoor[xxiv] equation under predicts the evaporation rate for low vapour pressure materials (toluene), and over predicts at high vapour pressures (n-hexane, n-pentane and Freon11).

In general, the average error for the three models was +57% for Phast 6.7, +23% for MacKay and Matsugu[xxiii] and +25% for Opschoor[xxiv]. This shows that Phast 6.7 gives by far the most conservative predictions, but MacKay and Matsugu[xxiii] and Opschoor[xxiv] equations largely improve the accuracy of the model for non-boiling evaporating pools. Overall MacKay and Matsugu[xxiii] is considered to provide the best results, while at the same time being conservative; as a result this option is selected to be the new default option in the new PVAP-MC standalone model.

Reijnhart and Rose[xvii] carried out experiments in a wind tunnel to investigate the dependency of the evaporation rate with respect to wind speed and surface roughness. Wind speed measurements were carried out at different vertical heights in the wind tunnel to obtain a wind velocity profile above the pool. All test runs for n-pentane and toluene at different roughness lengths were selected for the validation set. The following figures show the comparison between the three equations for evaporation (PVAP in Phast 6.7, MacKay and Matsugu[xxiii], Opschoor[xxiv]) and the experimental data from Reinhart and Rose[xvii]. Figure 5 contains the data for toluene at surface roughness lengths of $2.5 \cdot 10^{-3}$, 10^{-4} and $2.2 \cdot 10^{-5}$ m. Figure 7 presents the results for n-pentane at the highest surface roughness length, $2.5 \cdot 10^{-3}$ m. The results are presented in terms of the reduced evaporation rate (m^3/s) (see equation (5)) and the average wind speed across the boundary layer.

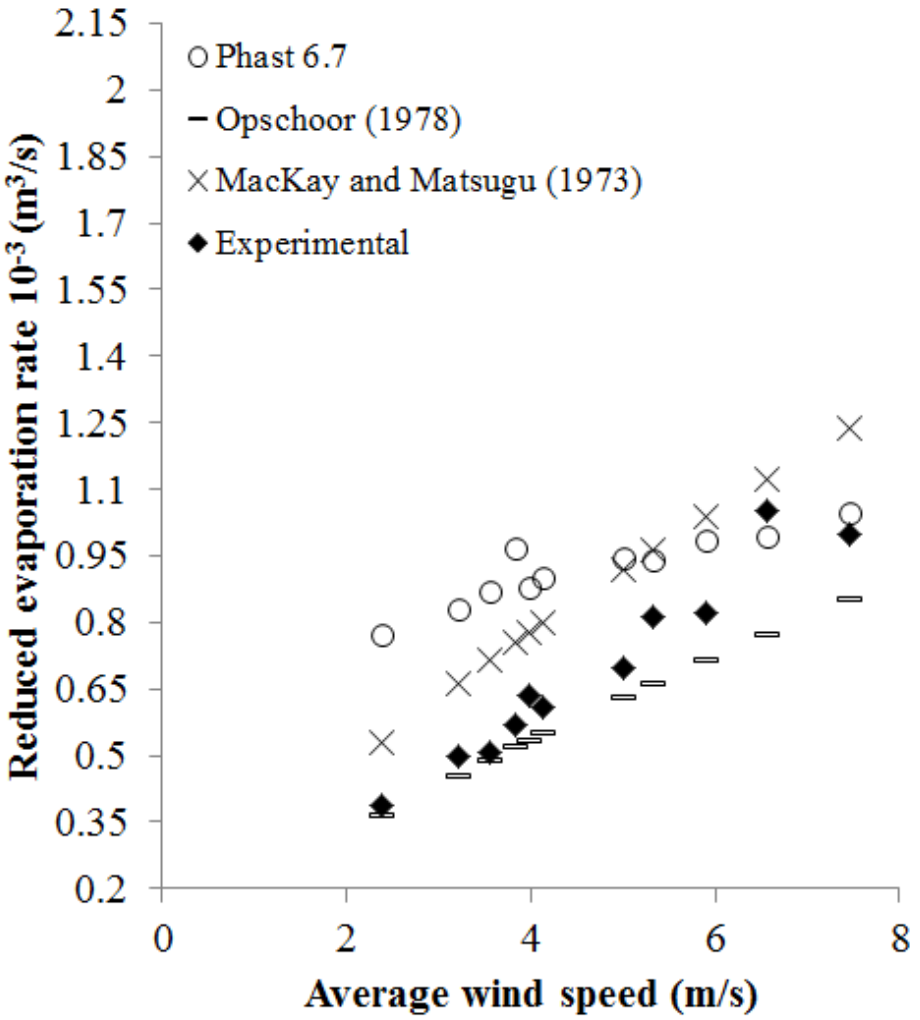

Figure 6 **Evaporation rate against average wind speed for toluene with roughness lengths of $2.5 \cdot 10^{-3}$, 10^{-4} and $2.2 \cdot 10^{-5}$ m. Comparison between models and experimental data (Reinhart and Rose[xvii]).**

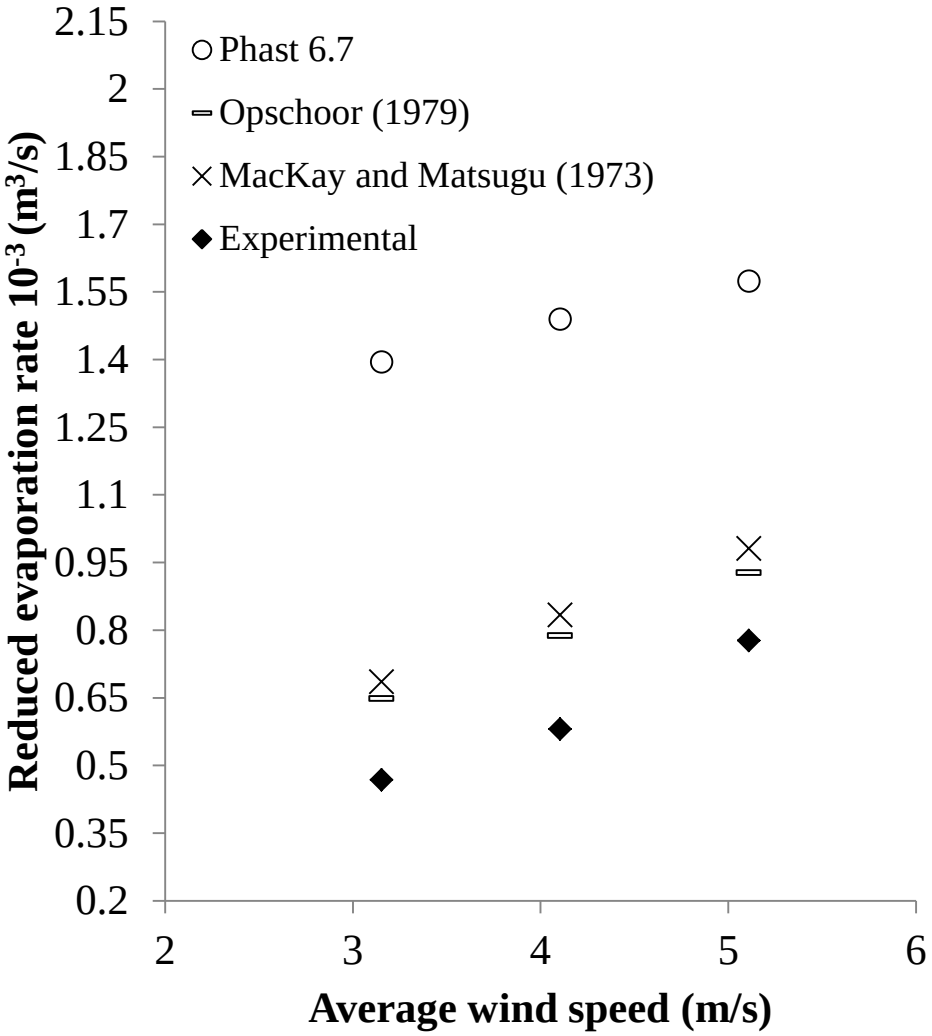

Figure 7 **Evaporation rate against average wind speed for n-pentane with a roughness length of $2.5 \cdot 10^{-3}$ m. Comparison between models and experimental data (Reinhjart and Rose[xvii]).**

From Figure 5, for toluene with different roughness length ($2.5 \cdot 10^{-3}$, 10^{-4} and $2.2\ 10^{-5}$ m), it can be observed that all three equations, Opschoor[xxiv], MacKay and Matsugu[xxiii] and Phast 6.7, show relative good agreement with the experimental data.

From the results shown in Figure 7, for n-pentane with a roughness length of $2.5 \cdot 10^{-3}$ m, it is observed that PVAP in Phast 6.7 greatly overpredicts the experimental data. MacKay and Matsugu[xxiii] and Opschoor[xxiv] equations present better agreement with the experiments.

In general, the percentage differences between model and experimental results are between -5 and +198% for Phast 6.7; between 7 and +46.5% for MacKay and Matsugu[xxiii]; and between -26 and +38.5% for Opschoor[xxiv]. The average differences between model and experimental data in absolute value are +67% for Phast 6.7, +30% for MacKay and Matsugu[xxiii] and +16.2% for Opschoor[xxiv].

Again, for this set of experimental data it is found that Phast 6.7 equation for evaporating pools is the most conservative of the three, but MacKay and Matsugu[xxiii] and Opschoor[xxiv] predict the evaporation rate for non-boiling pools with higher accuracy.

On the basis of the above comparisons between predicted and real data the MacKay and Matsugu[xxiii] formulation has been implemented as the default option for the calculation of non-boiling evaporating pools in the new PVAP model.

Norman and Dowell[xvi] performed a series of outdoor experiments with the intention of measuring the effectiveness of foams in suppressing chemical vapours from accidental spillages. Weight loss from a 0.9 m diameter pan was registered over a two hour period. Experiments were carried out in the presence and absence of foam layers of different thickness

over the pool surface. Very little data on the ambient conditions prevailing during the experiment is given, so caution should be exercised when comparing experimental and model data[5].

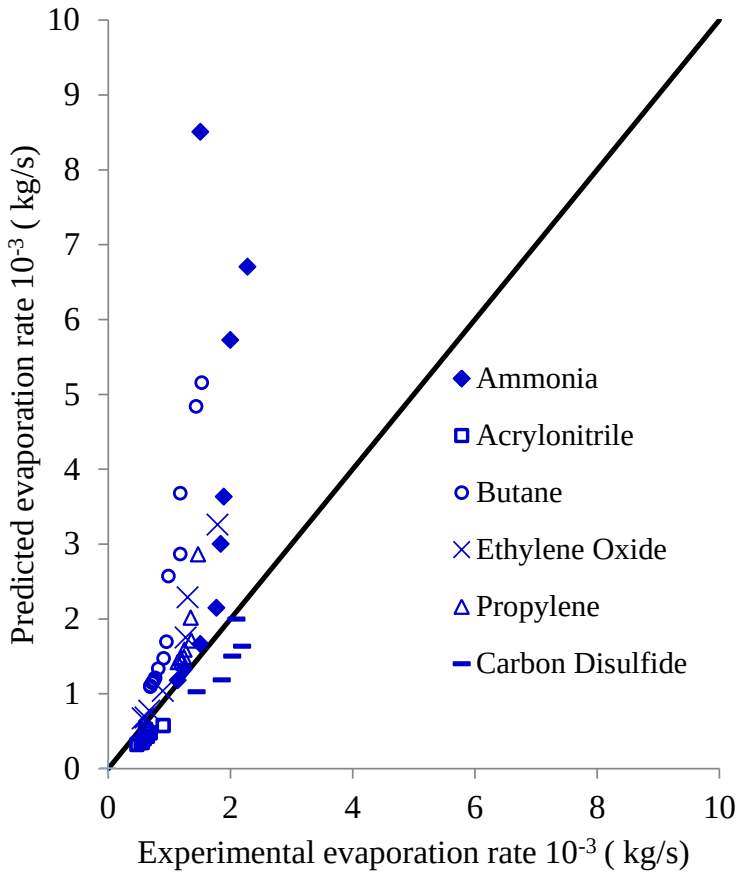

Figure 8 **Predicted against experimental (Norman and Dowell[xvi]) vaporisation rate for different chemicals on isolated surfaces**

As can be observed from Figure 8 PVAP and the experimental data do not present good agreement in some cases. For lower boiling point substances like ammonia and butane the agreement is worse than for less volatile materials such as ethylene oxide and carbon disulfide.

As mentioned above, the quality of this experimental data is questionable due to the lack of detail on the ambient conditions prevailing during the experiments, as the purpose of these experiments was not to measure the evaporation rate from pools, but to assess the degree of evaporation suppression of different foams arrangements.

Okamoto et al.[xiii] carried out a series of laboratory scale experiments to study the evaporation patterns of binary and ternary mixtures of n-Pentane, n-Hexane, n-Heptane, Toluene and p-Xylene at various compositions. The measurements were conducted under a fume hood. The fume hood fan was not operated, and the liquid evaporated under no wind condition. It should be noted that in the absence of wind the prevailing mass transfer mechanism between the pool and the air above it is natural convection. This poses a difficulty for the purpose of validation as the model assumes forced convection through a turbulent boundary layer. However, Okamoto et al.[xiii] carried out measurements of the mass transfer coefficients for pure components under the same conditions as the mixture studies. The mass transfer coefficients for pure components were determined from measurements of the evaporation rate and vapour pressures. Table 4 shows the experimental values obtained for n-Pentane, n-Hexane and n-Heptane.

Chemical	Mass transfer coefficient (10^{-4} m/s)
n-Pentane	3.64
n-Hexane	2.70
n-Heptane	2.63

Table 4 Experimental values for the mass transfer coefficients of hydrocarbon solvents (Okamoto et al.[xiii])

[5] The input data for the simulations has been extracted from an internal company document and the data has not been cross-checked against the original reference, therefore there is not a high level of confidence on the agreement between PVAP results and the experimental data

Figure 9 to Figure 11 show the predicted (curve A) and measured (curve B) pool evaporation rate against the weight loss fraction for binary and ternary mixtures of n-Pentane, n-Hexane and n-Heptane. The predicted evaporation rates are obtained from the mass transfer coefficients presented in Table 4 applying the following equation[6]:

$$E_{vap}(t) = \sum_{i=1}^{n} k^i \frac{M_c{}^i x_{pool}{}^i P_{vap}{}^i}{RT_{pool}} \quad (7)$$

Where, k^i are the experimental values for the mass transfer coefficient for each component presented in Table 4.

From the figures it is observed that the predicted and experimental data follow the same general trend. The model over-predicts the measured pool evaporation rate for weight loss fractions greater than 0.1, although it fails to account for the initially high rates of mass vaporised observed in the experiments. It should be noted that the experiments were carried out in the absence of wind, as Okamoto et al.[xiii] reported the fume hood fan was shut down while the mixtures were tested. In the absence of wind, it is likely that vapour will build up above the pool surface, increasing the concentration of the chemicals in the air and impeding the mass transfer from the liquid to the vapour phase. Thus, it is expected that measured evaporation rates will be lower than the predicted data as it is evidenced in the figures.

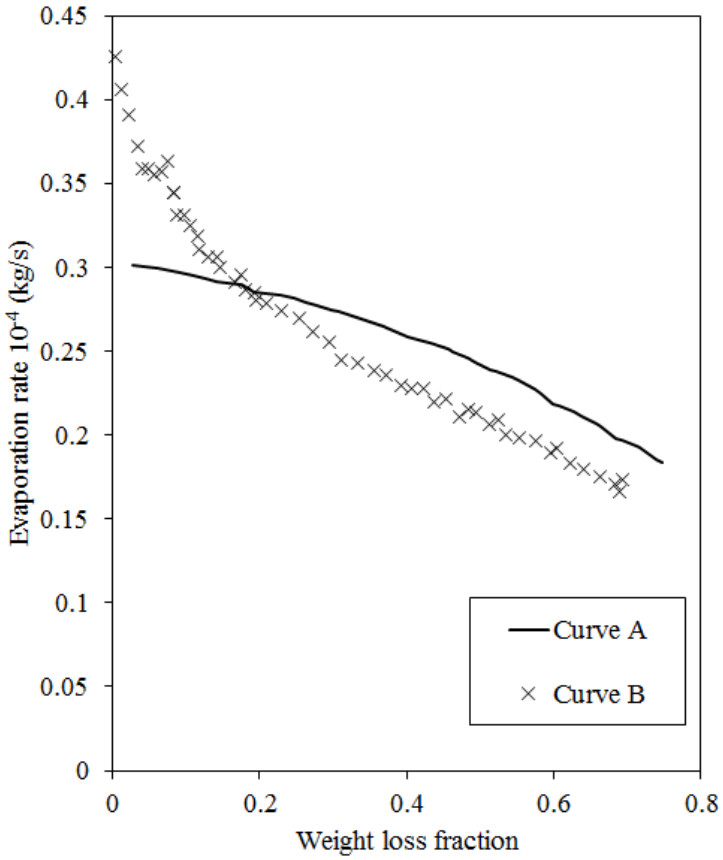

Figure 9 **Variation of the pool evaporation rate against the weight loss fraction for an n-Pentane/ n-Hexane instantaneous spill**
Curve A: Predicted data
Curve B: Experimental data (Okamoto et al.[xiii])

[6] As PVAP calculates the mass transfer coefficient according to the equations proposed by MacKay and Matsugu (1973) or Opschoor (1978), the predicted results presented here cannot be reproduced in PVAP.

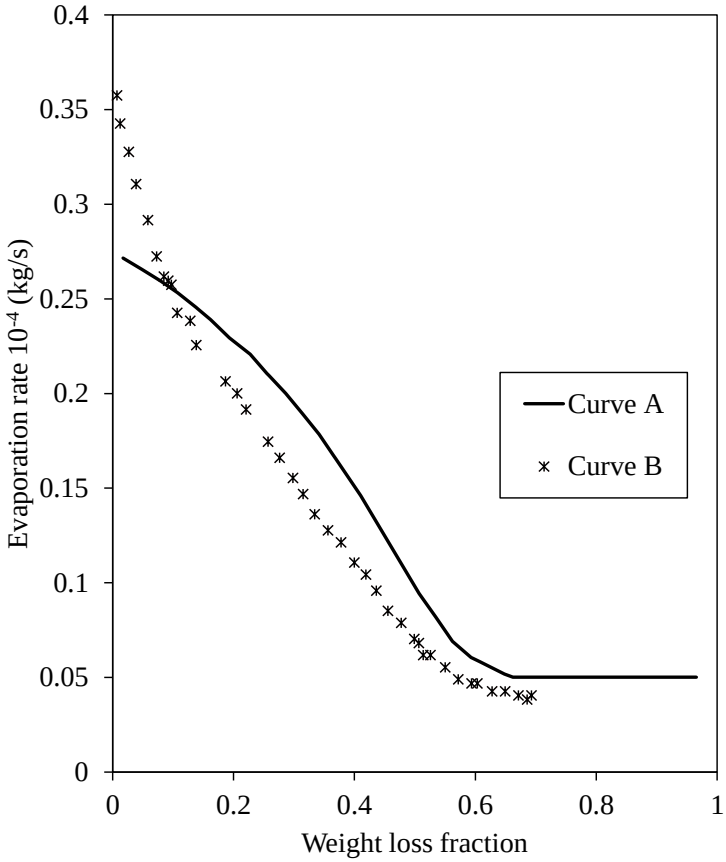

Figure 10 Variation of the pool evaporation rate against the weight loss fraction for an n-Pentane/ n-Heptane instantaneous spill
Curve A: Predicted data
Curve B: Experimental data (Okamoto et al.[xiii])

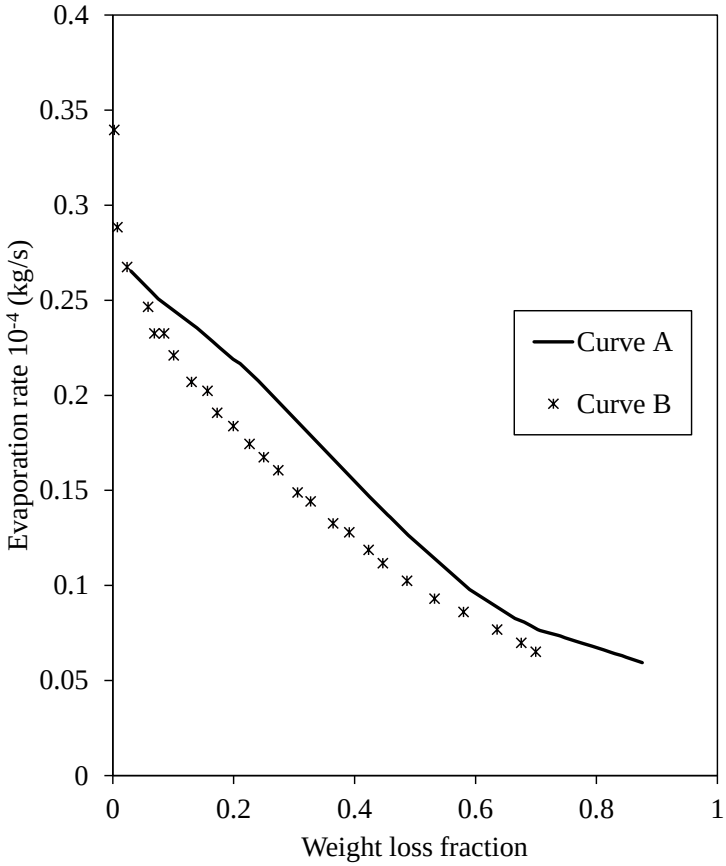

Figure 11 Variation of the pool evaporation rate against the weight loss fraction for an n-Pentane/ n-Hexane/ n-Heptane instantaneous spill
Curve A: Predicted data
Curve B: Experimental data (Okamoto et al.[xiii])

Habid et al.[xviii]: The set of experiments were carried out on the test facilities of the Federal Institute for Materials Research and Testing in Berlin (BAM). The set-up consisted of a circular basin of 0.74 m diameter which was insulated from the ground. The wind speed at a height of 2 m and the pool temperature were measured during the experiments. The wind speed at 10 m height was estimated using the power law for wind profiles with an exponent of 0.33 for very rough terrain, as reported by Habid et al.[xviii]. Fluctuations in the pool temperature were observed during the experiments and they were attributed to changes on the cloud cover according to Habid et al.[xviii]. The time-varying pool temperature was measured for the duration of the experiments, and these values were compared against the predicted values of PVAP.

The following figures show the results of the validation of PVAP predicted pool temperature against Habid et al.[xviii] experimental data and modelled data of Khajehnajafi and Pourdarvish[xxvi] from Safer Systems and Habid et al.[xviii] . The predicted data has been obtained using the MacKay and Matsugu[xxiii] correlation. From Figure 12 reasonable good agreement between the data predicted by PVAP and Safer Systems is observed; although Safer Systems model predicts an initial pool temperature which is lower than the measured value. It is also observed that the predicted pool temperature is much lower than the experimental data. Indicating that MacKay and Matsugu[xxiii] correlation under-predicts the time-varying pool temperature for cyclo-hexane on an insulated surface.

From Figure 13 it is also seen that the models under-predict the experimental data for an ethanol pool over an insulated surface. The results of PVAP are in relative good agreement with the model results of Habid et al.[xviii], but less so with the results predicted by Safer Systems.

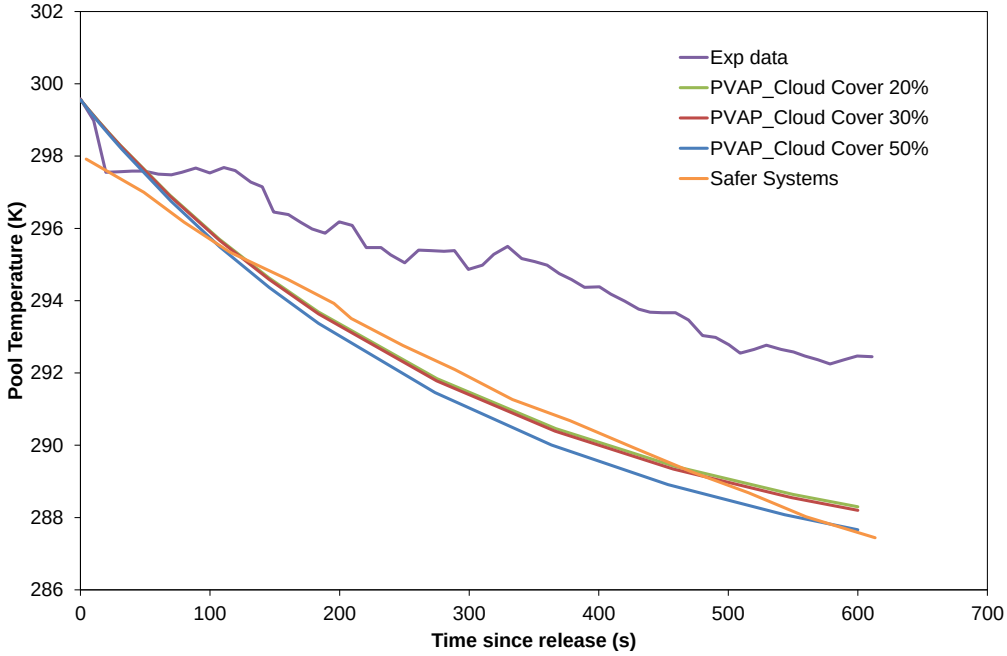

Figure 12. Predicted time-varying pool temperature validation for a cyclo-hexane pool on an insulated surface
Experimental data: Habid et al.[xviii]
Predicted data: PVAP at various cloud cover percentages
Predicted data: Safer Systems– MacKay and Matsugu[xxiii] correlation (Khajehnajafi and Pourdarvish[xxvii])
Wind speed at 10 m: 3.74 m/s; Spill mass: 5.27 kg; Spill temperature: 299.55 K

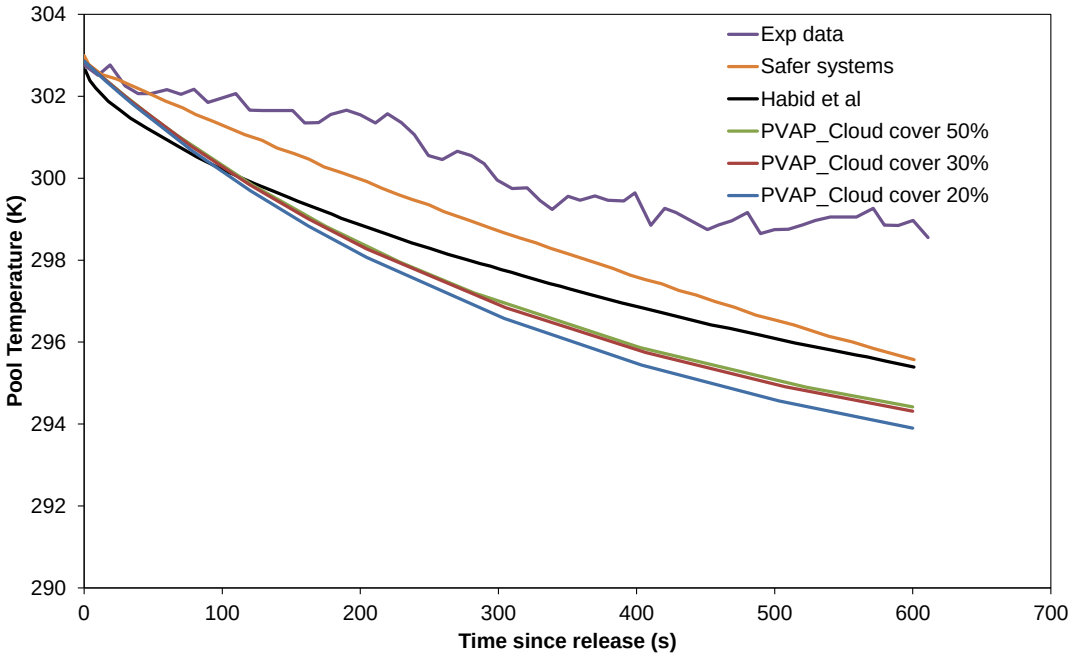

Figure 13. Predicted time-varying pool temperature validation for an ethanol pool on an insulated surface
Experimental data: Habid et al.[xviii]
Predicted data: Habid et al.[xviii] – MacKay and Matsugu[xxiii] correlation
Predicted data: PVAP at various cloud cover percentages
Predicted data: Safer Systems – MacKay and Matsugu[xxiii] correlation (Khajehnajafi and Pourdarvish[xxvii])
Wind speed at 10 m: 2.79 m/s; Spill mass: 5.14 kg; Spill temperature: 302.85 K

The authors also measured the initial and final mass in the pool, allowing for a rough estimate of the average pool evaporation rate. The table below compares PVAP predictions (using a cloud cover of 20%) against experimental results (Habid et al.[xviii]) for the averaged evaporation rate (kg/s), and it is seen that PVAP over-predicts the flow rate with 49% and 113%. Previous validation against Kawamura and MacKay[xv] cyclo-hexane experiments on sand also showed that PVAP over-predicted the experimental pool evaporation rate, in that case by 27%. Also previous verification against the GASP program indicated less cooling by GASP than for PVAP. This can be observed in Figure 14.

Material	Experiment (kg/s)	PVAP – 20% cover (kg/s)	% Over-prediction
Ethanol	3.57×10^{-4}	5.31×10^{-4}	49
Cyclohexane	6×10^{-4}	1.28×10^{-3}	113

Table 5. Average evaporation rate for ethanol and cyclohexane on an insulated surface

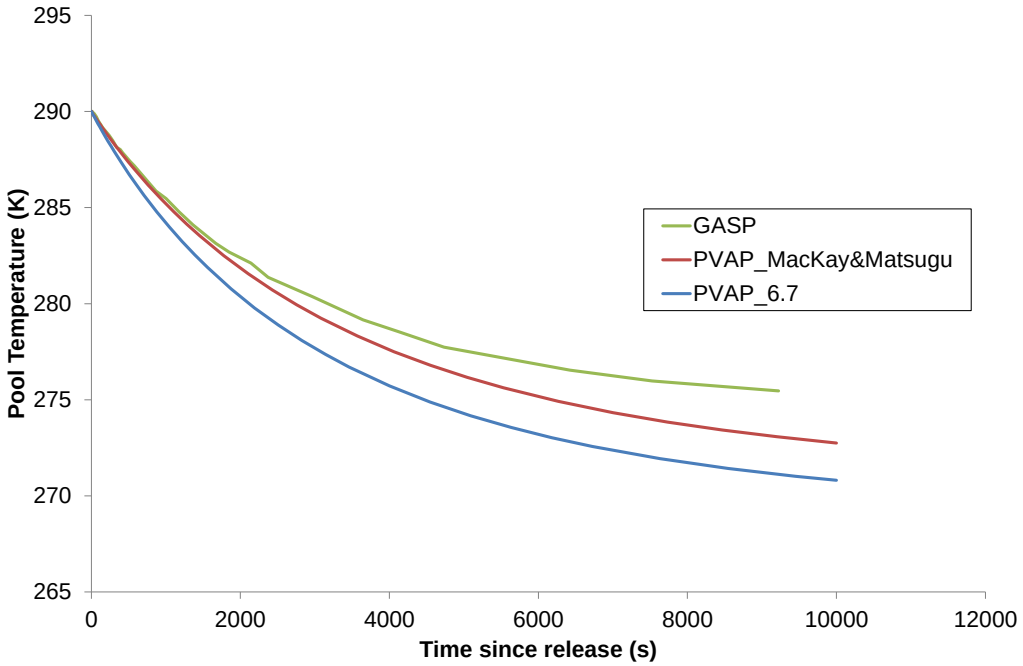

Figure 14. Comparison of the predicted time-varying pool temperature for an acrylonitrile pool on normal concrete
Predicted data: GASP
Predicted data: PVAP using MacKay and Matsugu[xxiii] evaporation equation
Predicted data: PVAP in Phast 6.7 and previous versions

3.1.3 Simultaneous pool spreading and vaporisation

Moorhouse and Carpenter[viii]: Very large scale LNG spill tests were carried out on three different surfaces, i.e. soil, concrete and steel and the pool radius variation over time was measured. Test runs on soil and concrete were selected for model validation. Figure 15 shows predicted against experimental pool radius for a continuous LNG spill on soil and concrete. The LNG spill was modelled as a spill of pure methane. While good agreement is found for soil, the model over predicts the maximum pool radius for a concrete surface. Moorhouse and Carpenter[viii] found better agreement with experimental data using a minimum thickness of 0.01 m for the concrete surface. This value is much higher than the default for concrete in PVAP (0.005 m). However PVAP over predicts the pool radius with a minimum thickness of 0.01 m as can be observed from Figure 15.

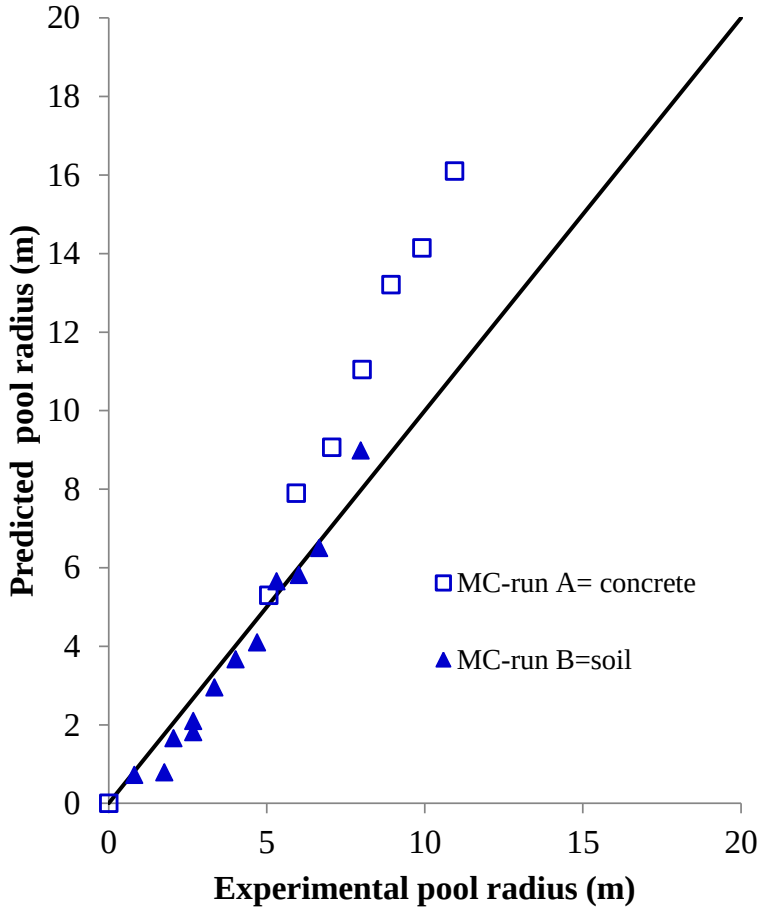

Figure 15 Predicted against experimental (Moorhouse and Carpenter[viii]) pool radius LNG– h_{min} = 0.01 m on concrete and soil

3.2 Pools on water

3.2.1 Pool spreading

Dodge et al.[xix] tested continuous and instantaneous spills of various hydrocarbons on a water basin. For continuous spill tests a centrifugal pump provided constant spill rates throughout the experiment. The chemicals were discharged vertically through a pipe at a height of 6.4 mm above the water surface. For instantaneous spill tests an open cylindrical tank without bottom was descended onto the surface of the water. The chemicals were metered into the tank and the cylindrical tank was raised allowing the pool to spill instantaneously. Pool radius measurements were taken at intervals of 0.3 and 0.6 m. Continuous and instantaneous spills of n-pentane and n-octane were chosen for the validation set.

Figure 16 compares the predictions of this model with the measurements for an instantaneous spill of 25.0 kg of pentane on water with a wind speed of 1.8 m/s. The fluid is assumed to be at an initial temperature of 25ºC, while a value of 20ºC is assumed for the ambient and water temperatures. Simulated results using minimum pool thicknesses (h_{min}) of 0m, 0.001m[7] and 0.0018m[8] are compared. In Figure 16 the pool spreading stops when the pool height reduces to the minimum thickness, i.e. at about 8s for h_{min}=0.0018, at about 20 seconds for h_{min}=0.001, and pool spread does not stop for h_{min}=0. It can be observed that using a value of the minimum pool thickness of 0.001m (i.e. "PVAP: h_{min}=0.001 (default)") provides improved model predictions as compared with 0.0018m (recommended value from Napier and Roopchard[xxviii]). In all, calculations made with the model described in this report are in good agreement with those of Dodge et al.[xix], and on average describe the experimental results well.

[7] This is the minimum pool thickness adopted in Phast 7.0 and earlier versions for simulating pool spreading on water

[8] This value corresponds to the minimum pool thickness recommended by the Purple Book and Napier and Roopchard (1986) for simulating pool spreading on water.

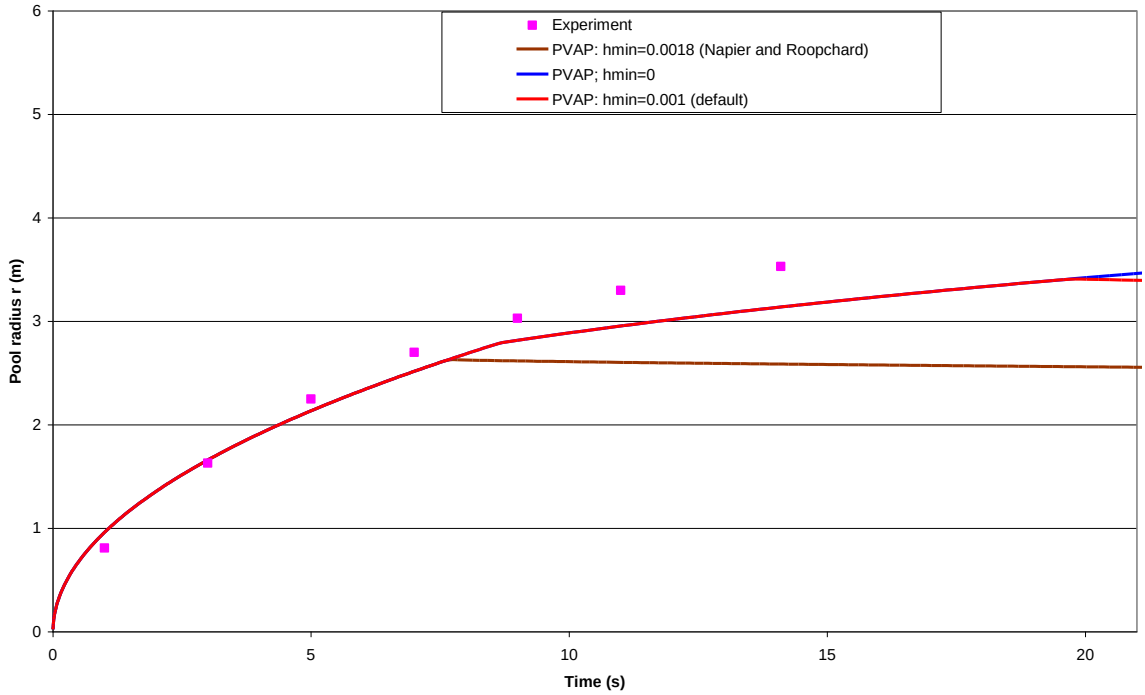

Figure 16 **Experimental data (Dodge et al.[xix]) and model calculation for an instantaneous spill of 25.0 kg of pentane on water with a wind speed of 1.83 m/s showing how the pool spreads when it is also simultaneously evaporating.**

Figure 17 presents predicted against experimental pool radius for pentane and octane spills on water. Good agreement is obtained for both instantaneous and continuous spills of n-pentane and n-octane.

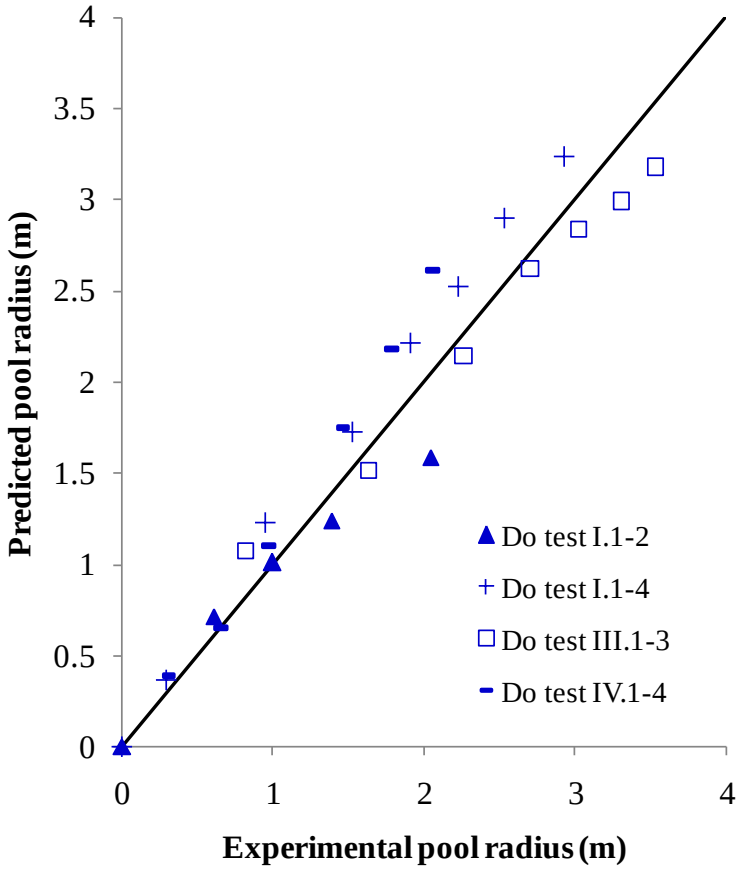

Figure 17 **Predicted against experimental (Dodge et al.[xix]) pool radius for a continuous (DoIV 1-4) and instantaneous (DoIII 1-3) n-pentane spill; and for a continuous (DoII 1-4) and instantaneous (DoII1-2) n-octane spill.**

3.2.2 Pool vaporisation

Bureau of Mines[ix] carried out a series of spill tests to further investigate the phenomena of Rapid Phase Transitions (RPTs) of LNG in contact with water. The substances tested were LNG, liquefied nitrogen and liquefied methane. The chemicals were spilt instantaneously from a tilting Dewar onto a water pond from a height ranging between 0.1 and 0.3 m. Experiments were repeated when covering the water pond with a 32 mm aluminium sheet. Pool weight loss was registered every 50 g. Evaporation rate data were derived for the duration of the test. PVAP was validated against the tests for pools on water only.

From Figure 18 it can be observed that PVAP results closely match the measured data up to 30 s after release. During this time the mass vaporized is mostly composed of Methane leading to the excellent agreement initially evidenced between the predicted results for Methane and the experimental data. After 30 s, lower vaporization is reported by the experiments as compared to the predicted values for Methane. This would indicate a decrease in the real inventory of Methane in the pool which results in an increase on the bubble point temperature and in the pool sensible heat, thus reducing the amount of energy available for vaporization. The results of the simulation for LNG follow the experimental trend for times greater than 40 s, but predict slightly higher values of the total mass vaporised, which could be attributed to mass losses during the experiment. Despite this, good agreement is observed between the LNG PVAP predictions and the measured data with an average deviation of +5%. The results of the Methane simulation are less accurate, although conservative, with maximum differences +of 10% with respect to the experimental data.

Figure 19 shows the predicted against experimental percentage of mass vaporised to mass spilled for methane and nitrogen spilled on water.

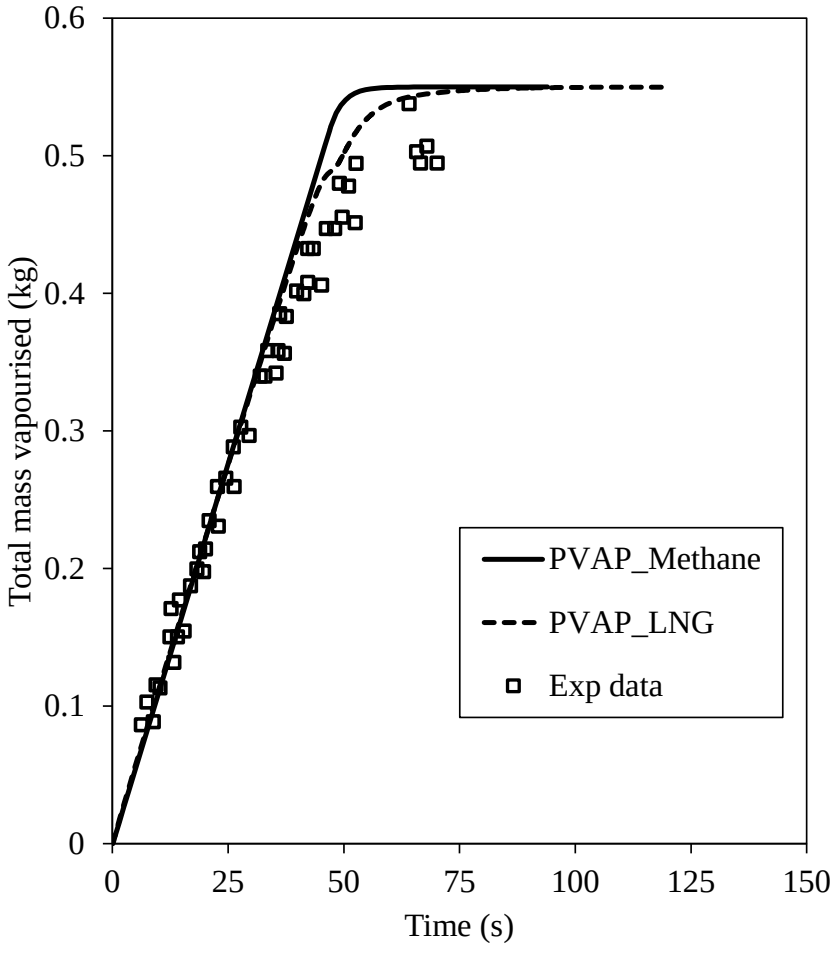

Figure 18 **Mass vaporised against time for experimental (Burgess et al.[ix]; BM18-34) and predicted (PVAP) data comparing methane and LNG simulations**

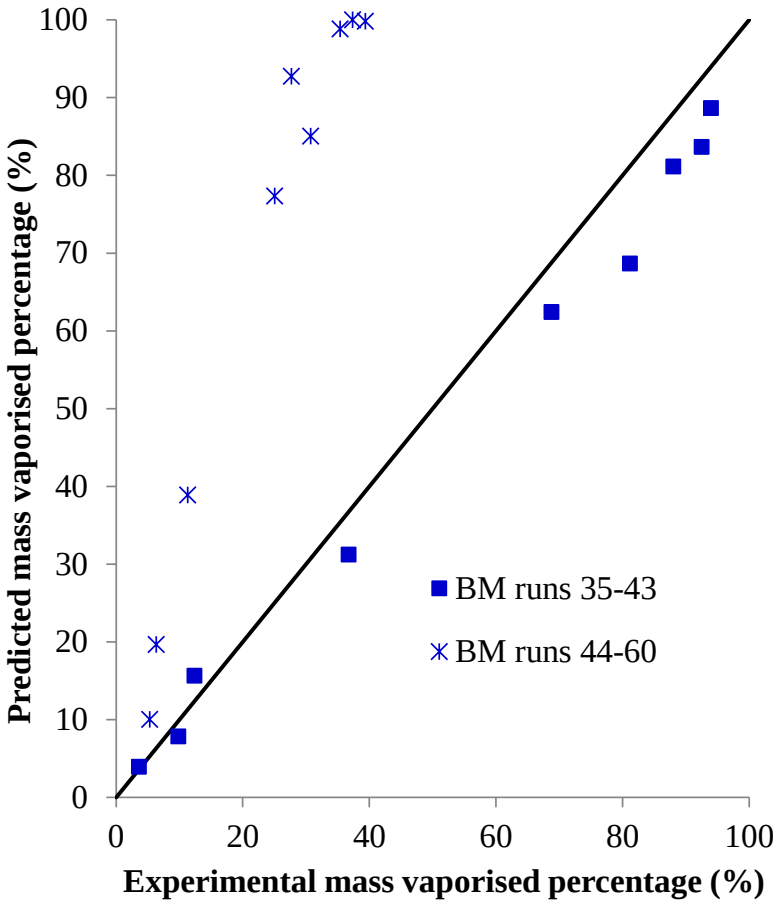

Figure 19 Predicted against experimental (Burgess et al.[ix]) percentage of mass vaporised for methane (runs 35-43 and nitrogen (44-60)

Good agreement is found for the methane tests (35 to 43). PVAP is shown to significantly over predict experimental data for the case of liquefied nitrogen (44 to 60). The reason for this could be the value given in PVAP to the heat transfer coefficient which is a material property. The stored value for nitrogen corresponds to the default (500 kW/m^2 obtained from data for n-butane spills on water (Reid and Smith[x])); however from this validation it is possible that the default value is unsuitable for nitrogen boiling on water[9].

Even though the scale of the experiment was not very large and could be considered a shallow water surface, the surface that provided the best fit to the experimental data was deep water.

LPG, ethane, ethylene and n-butane boiling behaviour was studied in an insulated calorimeter by Reid and Smith[x]. Instantaneous discharge of the chemicals was achieved by puncturing the rubber membrane bottom of a reservoir. Thermocouples recorded the temperatures of the evolved vapour and water. Pool weight over time was measured with a load cell. All test runs were included in the validation set. The data and calculations are compared in Figure 20 to Figure 22, which shows that a value of 500 W/m2/K for the heat transfer coefficient results in accurate predictions. Calculations also accurately reproduce the measured mass boiled off as a function of time for a confined, instantaneous spill of propane on ice.

Figure 21 shows the variation of the total mass vaporised against time for propane instantaneously spilled on water. The experimental data starts with an initial mass vaporised at time zero, corresponding to the mass lost during what Reid and Smith (1978) identified as an initial period of intense boiling. The authors did not provide a model or explanation to describe the boiling from this initial phase. For this experiment the authors observed that this initial period characterised by intense boiling lasted 3.6 s.

[9] A revision of the material properties for pools boiling on water has been carried as part of the Phast 6.7 work, however for Nitrogen no further experimental data have been found that can corroborate these results, and therefore the change to the material properties for nitrogen boiling on water has not been made.

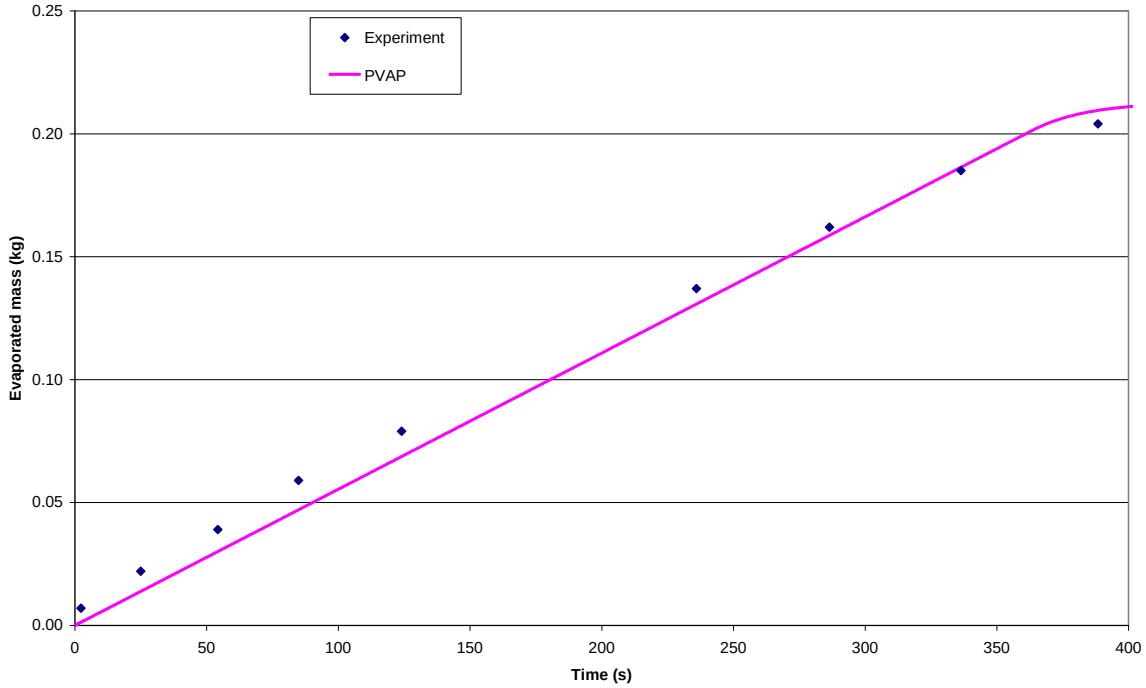

Figure 20 **Experimental data (Reid and Smith[x]) and model calculations for the instantaneous spill of butane into a confined volume of water**

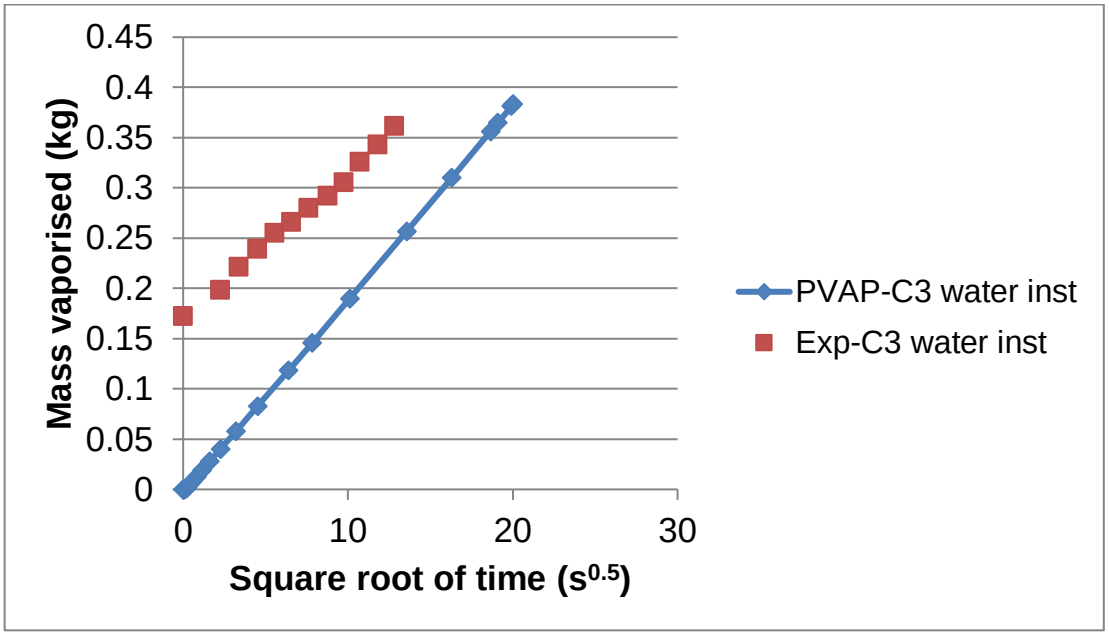

Figure 21 **Experimental data (Reid and Smith[x]) and model calculations for the instantaneous spill of propane into a confined volume of water[10]**

[10] The initial intense boiling regime observed by Reid and Smith (1978) for boiling propane on shallow water (including ice formation) was not observed for similar instantaneous releases of boiling LNG on deep water (Burgess et al.1972) (without ice formation). Further investigation of this may explain the under-predictions of PVAP-MC for the initial intense boiling regime

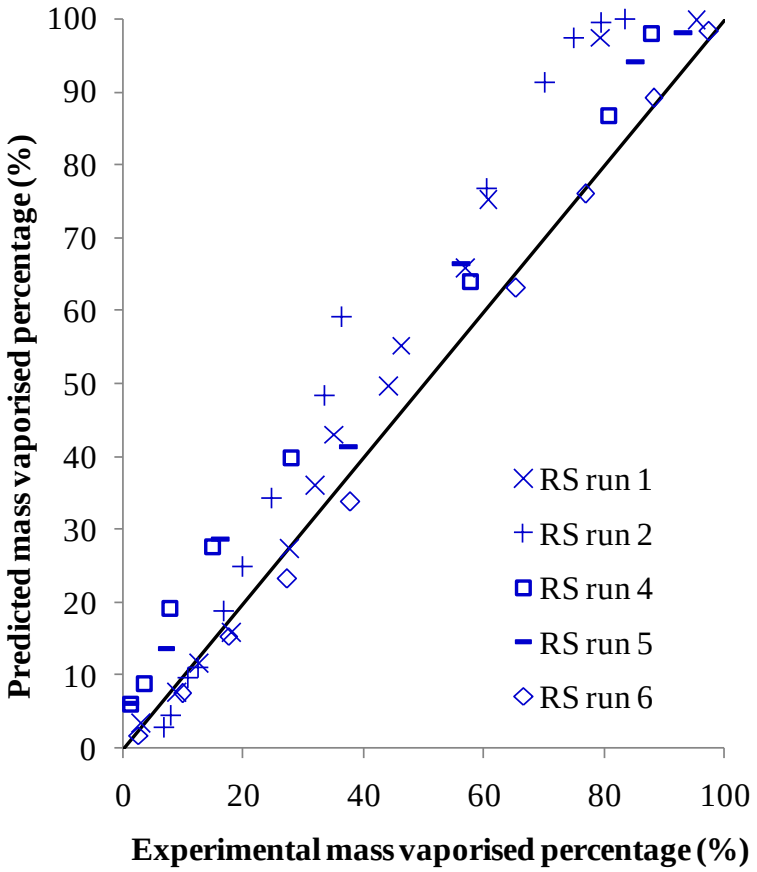

Figure 22 **Predicted against experimental (Reid and Smith[x]) percentage of mass vaporised for propane on ice (run 1), LPG on water (run 2), ethane on water (run 4), ethylene on water (run 5), butane on water (run 6)**

3.2.3 Simultaneous pool spreading and vaporisation

Koopman et al.[xi] carried out the Burro series of experiments, where LNG was spilled onto a water basin with an average diameter of 58 m and a depth of 1 m. The spill plate was located just below the water surface, to feed the LNG horizontally onto the basin surface. Concentration measurements were obtained from sensors arrayed into arcs at 100, 140, 400 and 800 m downwind from the release point. The majority of the data made available for the Burro series experiments concerns runs 8 and 9, which were selected for the model to be compared against. Figure 23 shows the predicted against experimental percentage mass vaporised to mass spilled for LNG continuously spilled on water.

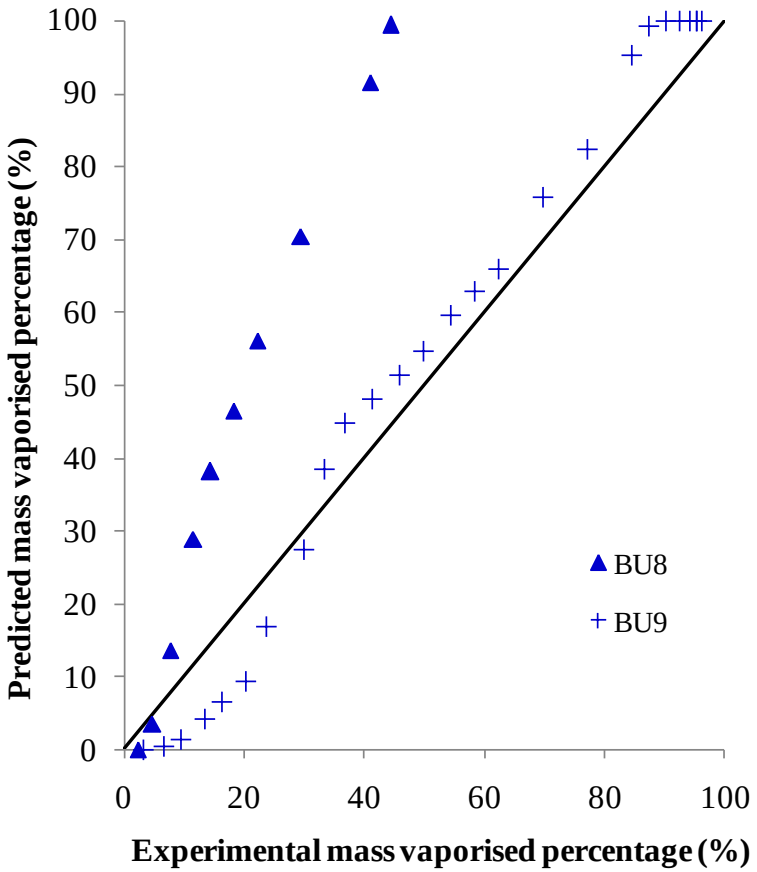

Figure 23 Predicted against experimental (Burro series[xi]) percentage of mass vaporised for a continuous spill of LNG

Cumulative mass vaporised against time was reported by the authors based on measurements at 400 m from the centre of the spill. The authors reported a mass loss corresponding to 28% and 24% of the spill for Burro 8 and 9, respectively, at the point where the measurements were made. The results presented in the above figure take this mass loss into account. The comparisons of the variation of the predicted and experimental mass vaporised against time for Burro 8 and 9 are in Figure 24 and Figure 25 respectively.

The good agreement observed in the validation against Burro 9 (Figure 25) was not reproducible in Burro 8 (Figure 24). Comparing the experimental data of Burro 8 and 9 it can be seen that Burro 8 was observed to vaporise twice as slow as Burro 9. In Burro 8 the spill rate was lower than in Burro 9, therefore the pool will grow at a slower pace in Burro 8 affecting the vaporisation rate over the pool surface area. This behaviour was not reflected by PVAP and could be attributed to the conservative pool spreading on water model. For both Burro 8 and 9, PVAP gives conservative estimates.

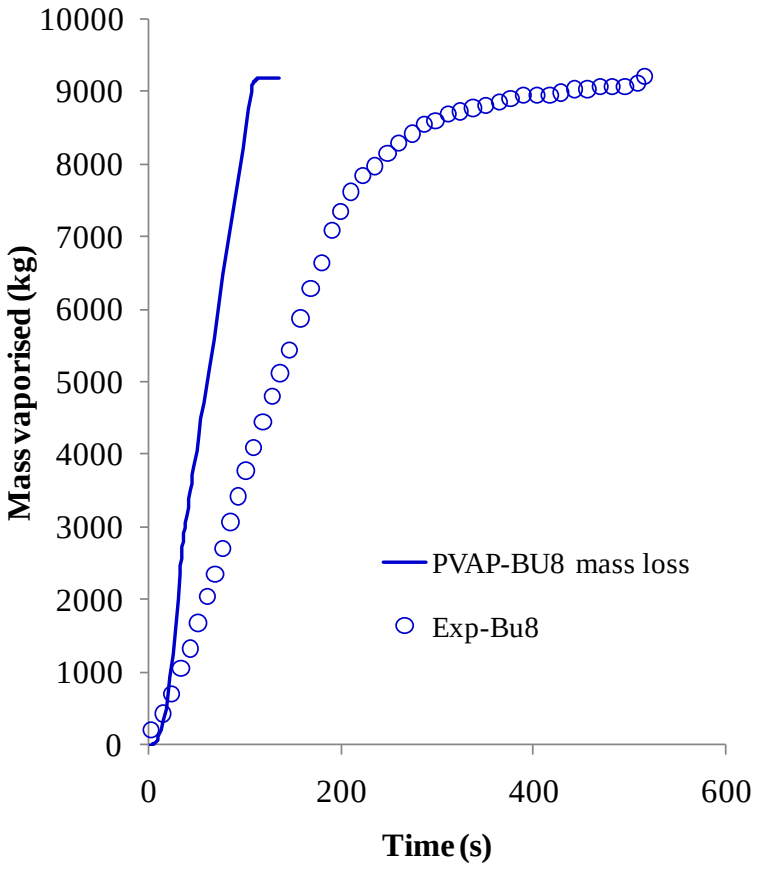

Figure 24 **Comparison between predicted and experimental (Burro series[xi]) mass vaporised for a continuous spill (112 kg/s for 107s) of LNG on shallow water considering a mass loss of 28%**

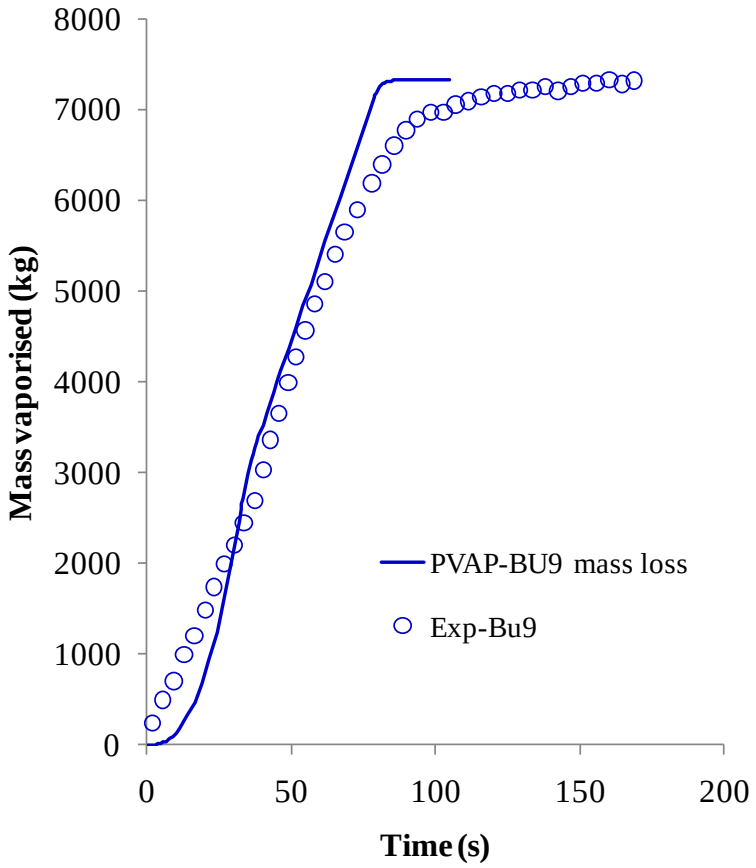

Figure 25 Comparison between predicted and experimental (Burro series[xi]) mass vaporised for a continuous spill (130 kg/s for 79 s) of LNG on shallow water considering a mass loss of 24%

Burgess et. al.[xxix] spilled LNG and liquid nitrogen onto fresh water, salt water, and ice in order to investigate the boil-off and liquid spreading rates. Both the maximum diameter of the pool and the time for almost complete vaporisation were measured. Our calculations somewhat under-predict the maximum diameter and over-predict the duration, particularly for the smallest spills. ESSO (Feldbauer et al.[xxx]) carried out a total of 17 LNG spill tests. Run 12 involved the continuous release of 415 kg of LNG over a 6 s time period. It was observed that the pool spread for 11 s achieved a maximum diameter of 14 m. Calculations with our model predict that the pool would spread for 15 s to a maximum diameter of 18.5 m[11].

3.2.4 Validation of spills of ammonia on water

Raj and Reid[xii] describe the results of an experimental program to determine the fraction of ammonia which dissolves when spilt on water. It was found that about 0.6 to 0.7 of the ammonia which is spilt dissolves into the water, this fraction not being significantly dependent on the mode or size of spill, salinity, water temperature, water depth, etc. To test if the ammonia-water reaction model as implemented here is consistent with these experimental measurements a number of calculations were carried out for instantaneous spills of different sizes, continuous spills of different release rates and durations, and different water temperatures. For all cases simulated, the following assumptions are made:

- The water and ambient temperatures are the same
- The prevailing wind speed at 10m reference height is 1m/s
- Solar radiation flux is 0 W/m^2
- Ammonia is released on a deep open pool of water at its boiling point (i.e. 239.72K)

The adopted input data and results of the simulation are presented in
Table 6,
Table 7 and

[11] These calculations were conducted using an earlier version of PVAP. As such, simulated results using the present version and related observations and/or conclusions may differ. These experiments have not been reproduced as the reference (Thyer, 1996) does not provide enough detail

Table 8. In all cases the maximum fraction of ammonia calculated to dissolve was about 0.7 (i.e. the partition coefficient). This is consistent with the experimental results. However, due to the effect of heat source terms[12] other than the dissolution term (i.e. Q_{sol}) the real fraction dissolved is lower than the calculated maximum. The difference between 1 and the sum of "fraction evaporated due to dissolution only" and "fraction dissolved" should approximately equal the fraction evaporated due to other heat source terms.

Spill Mass [kg]	Partition Coefficient [-]	Fraction Dissolved [-]	Fraction Evaporated due to dissolution only [-]
1	0.6923	0.612	0.307
10	0.6923	0.614	0.307
100	0.6923	0.614	0.307
1000	0.6923	0.614	0.307
10000	0.6923	0.615	0.307
100000	0.6923	0.615	0.307

Table 6 Input data and results for the spreading and vaporisation of instantaneous ammonia spills on water (water temperature fixed at 288K)

Water Temperature [K]	Partition Coefficient [-]	Fraction Dissolved [-]	Fraction Evaporated due to dissolution only [-]
278	0.7211	0.629	0.278
288	0.6923	0.614	0.307
298	0.6606	0.594	0.339

Table 7 Input data and results for the spreading and vaporisation of instantaneous ammonia spills on water (Spill mass of 1000kg)

Spill Rate [kg/s]	Duration [s]	Partition Coefficient [-]	Fraction Dissolved [-]	Fraction Evaporated due to dissolution only [-]
1	1000	0.6923	0.616	0.307
10	100	0.6923	0.615	0.307
100	10	0.6923	0.615	0.307
1000	1	0.6923	0.615	0.307

Table 8 Input data and results for the spreading and vaporisation of continuous ammonia spills on water

Additionally, the pool model results of a study case for an instantaneous spill of 100 kg of ammonia on a water surface at 294 K are compared to the original results of the Raj and Reid[xii] model in Figure 26. Both the original data of Raj and Reid[xii] and the pool model results are in line with the experimental data in that after the partition coefficient has been reached further addition of water to the pool won't result in further evaporation.

[12] i.e. Q_{rad}, Q_{conv}, Q_{cond}

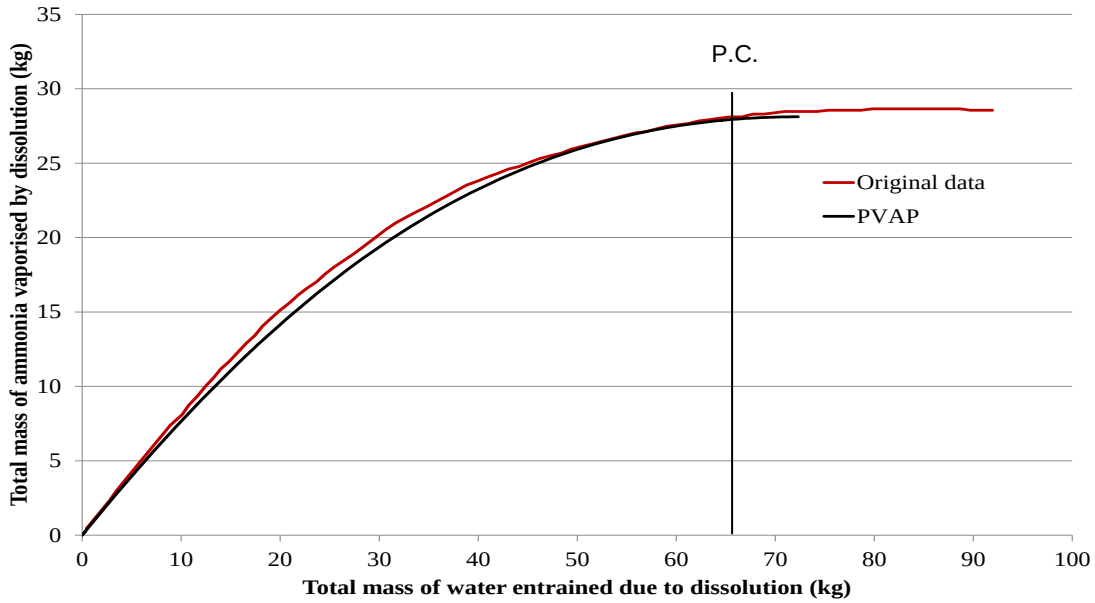

Figure 26 Mass of ammonia vaporised by dissolution vs mass of water entrained

3.3 Summary

From the validation presented above the following conclusions may be reached:

- The spreading on land model gave maximum deviation of +50% with respect to the experimental data.
- Boiling on land model show good agreement with the experimental data.
- Validation of evaporation on land models showed better agreement between predicted and experimental data for MacKay and Matsugu[xxiii] equation and therefore it has been selected as the new default option for the new standalone PVAP model in Phast.
- Simultaneous spreading and vaporisation on land models presented agreement within 30% of the experimental results.
- Boiling on water model showed agreement within 20% of the experimental data for hydrocarbons; higher deviations of up to +50% were obtained for nitrogen.
- The spreading on water model show good agreement with the experimental data, instantaneous spills were found to give closer predictions to the real data than continuous spills
- Simultaneous spreading and vaporisation on water models were found to be too conservative with respect to the experimental data.
- The reactive ammonia on water model was found to predict well the experimental data

4 FUTURE WORK

This section presents the future work on the validation for PVAP as well as future improvements to the model based on the results presented in this document.

Future work on the model validation includes:

- Carry out further validation of PVAP predictions of pool temperature and evaporation rate for non-boiling pools
- Provide further quantitative measure of the level of agreement of PVAP results against experimental data

The validation presented in this document also had the purpose of pinpointing areas of future improvements to the model. The following list shows possible future improvements to the model divided into two sections, pool spreading and pool vaporisation, the latter includes heat and mass transfer models.

4.1 Pool spreading

- From the validation against Belore and McBean[xiv] and Moorhouse and Carpenter[viii] experiments the impact of the minimum thickness on the pool spreading behaviour was shown. The values for the minimum pool thickness h_{min} are available for a range of surfaces in PVAP. The values for h_{min} are also dependent on the physical properties of the liquid such as surface tension σ_L, viscosity μ_L and liquid density ρ_L. A lower bound for the minimum thickness can be the capillary depth $h_c = (\sigma_L/g\rho_L)^{1/2}$. However this value may be too low, and thus leads to pools with a very large area. Additionally, for not perfectly smooth surfaces the pool is expected to reach its maximum area before reaching the capillary depth, due to the surface roughness. Therefore, the surface roughness length of the material should be the controlling parameter. Following the steady-state model of Webber[xxxi xxxii], one could suggest for slowly-varying release rates to take h_{min} variable as function of the time t, i.e. to take $h_{min} = h_{min}(t) = \max[h_c, (6\nu_L S(t)/\pi g)^{1/4}]$, where S(t) is the spill rate at the present time t. For instantaneous releases the surface roughness length may provide the best estimate for h_{min} (Van den Bosch[xxi]). A comparison on updated values for the surface roughness length from more recent literature is required.

- After the pool has reached the minimum thickness and continuous to lose mass by evaporation or dissolution, the mass conservation principle forces the radius of the pool to shrink. In reality, the pool will break up into a number of separate blobs, instead of simply shrinking, of thickness equal to the minimum thickness. The simplistic nature of the model assumes that properties are constant along the length of the pool, and mass and heat transfer coefficients are calculated as area averages. As it is, a shrinking pool, although an unrealistic scenario, won't have an effect on the other pool variables (e.g.: vaporisation rate, temperature) for the purposes of modelling.

- Dodge et al.[xix] model for spreading of pools on water adopts the spill mass and spill rate for instantaneous and continuous releases, respectively. The experiments carried out by Dodge et al.[xix] were limited to materials with relative low volatility, e.g: pentane, octane and kerosene, so good agreement between model and experiments was expected. Validation of simultaneous boiling and spreading models against Burro series[xi] of experiments showed PVAP to give conservative estimates of the mass vaporised over time.

  The substitution of the spill mass with the pool variable mass may not provide the optimal solution, because of the fitting of the equation constants to experimental data. Additionally, the model provides explicit equations for the pool radius instead of a spreading law of the form dr/dt. This formulation is derived from the assumption of the pool acceleration to be equal to $r/2t^2$. Following Webber and Jones[xxxiii] a model with two differential equations du/dt and dr/dt may be suggested will avoid the assumption made for the du/dt in Dodge et al.[xix].

4.2 Pool vaporisation

- From the validation against Reid and Wang[vii] LNG experiments on soil and concrete, a comparison with updated values from the literature for the surface thermal properties, e.g. thermal conductivity and diffusivity is suggested.

- From the comparison of simulated results of PVAP in Phast 6.7, MacKay and Matsugu[xxiii] and Opschoor[xxiv] equations against the Kawamura and Mackay[xv], Reijnhart and Rose[xvii] and Norman and Dowell[xvi] data sets it is suggested to use the MacKay and Matsugu[xxiii] equation for the heat of evaporation.

- The validation carried out showed little evidence of ice formation on experiments carried out on water, even at medium, small scale experiments (see validation against Bureau of Mines[ix] LNG and methane experiments, and Reid and Smith[x] n-butane experiments). It may be suggested thus to give the choice to the user to enable/disable the ice formation option.

- The conductive heat on land formula may be improved by implementing the formulations proposed by Webber[xxxiv] or Leonelli[xxxv] for a pool that spreads and vaporises at the same time. Currently, PVAP uses an approximation to this formula following the work of Shaw and Briscoe[xxxvi]. Moorhouse and Carpenter[viii] sets of experiments measure simultaneous spreading and vaporisation of LNG. As was discussed in section 4.1.3 good agreement was obtained for LNG boiling and spreading on soil but not on concrete. After values of the minimum thickness have been updated according to more recent literature (section 5.1), and the agreement with Moorhouse and Carpenter[viii] is not satisfactory, the formulation of the heat of conduction on land should be improved.

APPENDICES

Appendix A. Input data for validation runs

The following tables indicate the input parameters for PVAP validation runs. Default data are applied except for the cut-off rate for the evaporation rate until which the PVAP simulations needs to be carried out.

Table A 1. Common and default input parameters of PVAP

Parameter	Value	Default
Ambient, material and surface parameters		
Atmospheric molecular weight (kg/kmol)	28.966	
Atmospheric heat capacity (J/kg/K)	1004	
Concentration power for toxic load calculation (-)	1	
Model flags		
Bund overspill flag (0- Off 1- On)	0	
Wind speed profile flag (1- Constant, 2- Logarithmic)	2	
Solver flag (1-Runge Kutta, 2-Non stiff, 3-Adaptive)	2	
Limits		
Cut-off height for wind speed calculation (m)	1	
Cut-off pool evaporation rate (kg/s)	10^{-7}	10^{-3}
Minimum temperature (K)	9.99	
Accuracy and output control		
Solver tolerance	10^{-3}	
Maximum number of pool segments	10	
Maximum array size	1000	
Record length of results file	50	
Index of next result records to write file to	1	

A.1 Pools on land

Series		**Belore and McBean**	
Spill		Continuous	
Substance		Water	
Spill temperature (K)		295	
Pasquill stability class		F (stable)	
Reference height for wind speed (m)		10	
Wind speed at reference height (m/s)		0.1001	
Atmospheric temperature (K)		295	
Solar radiation (W/m^2)		0	
Type of surface		Plywood-User defined	
Surface roughness factor		1	
Thermal conductivity (W/m.K)		0.12	
Thermal diffusivity (m^2/s)		$1.81 \cdot 10^{-7}$	
Minimum thickness (m)		5.10^{-3} and 10^{-2}	
Surface temperature (K)		295	
Maximum simulation time (s)		80	
BMB28	**BMB29**	**BMB30**	
0.367	0.8028	1.218	Spill rate (kg/s)
80	60	60	Spill duration (s)

- Surface and spill temperature not provided by the author, set to atmospheric temperature (295 K).
- Plywood thermal conductivity and thermal diffusivity taken from Rohsenow et al.[xxxvii].

Series		**Reid and Wang**		
Substance		Methane		
Spill		Instantaneous		
Spill duration (s)		0.001		
Spill temperature (K)		111.7		
Pasquill stability class		F (stable)		
Atmospheric temperature (K)		293.15		
Wind speed (m/s)		.1001		
Reference height for wind speed (m)		10		
Solar radiation (W/m^2)		0		
Bund diameter (m)		0.357		
Surface temperature (K)		280		
Maximum simulation time (s)		3000		
Soil roughness factor		2.63		
Soil thermal conductivity (W/m.K)		6		
Soil thermal diffusivity (m^2/s)		$3.41 \cdot 10^{-5}$		
RW70	**RW21**	**RW40**	**RW41**	
20	0.485	0.663	0.429	Spill mass (kg)
Concrete	Soil- RW	Soil- RW	Soil- RW	Type of surface
$5 \cdot 10^{-3}$	10^{-7}	10^{-7}	10^{-7}	Minimum thickness (m)
RW42	**RW44**	**RW45**	**RW47**	
0.669	0.847	1.23	0.645	Spill mass (kg)
Soil- RW	Soil- RW	Soil- RW	Soil- RW	Surface
10^{-7}	10^{-7}	10^{-7}	10^{-7}	Minimum thickness (m)

- Values of soil thermal conductivity and diffusivity taken from Reid and Wang[vii].
- Minimum thickness set to 10^{-7} m due to the small scale of the experiment. As spreading is not under study here, the results remain unaffected.
- Atmospheric data not provided by the authors, scale of the experiments indicate they were carried indoors. Default values for indoor experiments were selected as input.

Series		**Moorhouse and Carpenter**
Substance		Methane
Spill		Continuous
Spill temperature (K)		111.66
Pasquill stability class		D (neutral)
Atmospheric pressure (Pa)		101,325
Reference height for wind speed (m)		10
MC-A	**MC-B**	
64.35	52.56	Spill rate (kg/s)
300	175	Spill duration (s)
350	50	Solar radiation (W/m^2)
293.15	290.15	Atmospheric temperature (K)
4.48	2.64	Wind speed at reference height (m/s)
$5 \cdot 10^{-3}$	10^{-1}	Surface roughness length (m)
Concrete	Dry soil	Type of surface
293.15	289.15	Surface temperature (K)
300	175	Maximum simulation time (s)

- Atmospheric stability class not given, outdoor default values used.

Series	**Kawamura and MacKay**
Spill	Instantaneous
Spill duration (s)	0.001
Pasquill stability class	D (neutral)
Atmospheric pressure (Pa)	101,325
Reference height for wind speed (m)	10
Bund diameter (m)	0.46
Type of surface	Sand-user defined
Surface roughness factor	2.6
Thermal conductivity (W/m.K)	2.08
Thermal diffusivity (m^2/s)	$7 \cdot 10^{-7}$
Minimum thickness (m)	10^{-7}
Vaporisation cut-off rate (kg/s)	10^{-7}

KM18	**KM20**	**KM21**	**KM22**	
Toluene	N-hexane	N-Pentane	N-Pentane	Substance
3.46	2.62	4.37	2.49	Spill mass (kg)
298.15	300.15	296.15	298.15	Spill temperature (K)
872	728	647	861	Solar radiation (W/m^2)
298.15	300.15	296.15	298.15	Atmospheric temperature (K)
2.65	1.59	4.94	5.42	Wind speed (m/s)
298.15	300.15	296.15	298.15	Surface temperature (K)
1260	540	385	209	Maximum simulation time (s)
		KM19	**KM23**	
		Cyclo-hexane	Freon 11	Substance
		3.08	10.24	Spill mass (kg)
		302	295	Spill temperature (K)
		894	853	Solar radiation (W/m^2)
		302	295	Atmospheric temperature (K)
		3.14	1.17	Wind speed (m/s)
		302	295	Surface temperature (K)
		6000	5400	Maximum simulation time (s)

- Minimum thickness set to 10^{-7} m due to the small scale of the experiment. As for Reid and Wang[vii].
- The surface roughness factor, which corrects the area for heat transfer between the surface and the pool to account for unevenness, is assumed to be similar to the value in PVAP's database for dry and wet soil.
- Sand thermal conductivity and diffusivity taken from Kawamura and MacKay[xv].

Series	**Reijnhart and Rose**
Spill	Instantaneous
Spill duration (s)	0.001
Spill mass (kg)	10
Temperature of the spill (K)	293.15
Pasquill stability class	F (stable)
Atmospheric temperature (K)	293.15
Solar radiation (W/m2)	0
Bund diameter (m)	0.28
Surface temperature (K)	293.15
Maximum simulation time (s)	3000
Surface roughness factor	1
Surface thermal conductivity (W/m.K)	0.1
Surface thermal diffusivity (m^2/s)	$1 \cdot 10^{-8}$

RR-1	**RR-2**	**RR-3**	
Toluene	Toluene	Toluene	Substance
$2.5 \cdot 10^{-3}$	$2.5 \cdot 10^{-3}$	$2.5 \cdot 10^{-3}$	Surface roughness length (m)
6.03	7.80	9.16	Wind speed (m/s)
10	10	10	Reference height for wind speed (m)
RR-4	**RR-5**	**RR-6**	
n-Pentane	n-Pentane	Pentane	Substance
$2.5 \cdot 10^{-3}$	$2.5 \cdot 10^{-3}$	$2.5 \cdot 10^{-3}$	Surface roughness length (m)
5.00	6.44	7.94	Wind speed (m/s)
10	10	10	Reference height for wind speed (m)

RR-7	**RR-8**	**RR-9**	**RR-10**	
Toluene	Toluene	Toluene	Toluene	Substance
$1 \cdot 10^{-4}$	$1 \cdot 10^{-4}$	$1 \cdot 10^{-4}$	$1 \cdot 10^{-4}$	Surface roughness length (m)
5.62	6.49	7.79	9.11	Wind speed (m/s)
10	10	10	10	Reference height for wind speed (m)
RR-11	**RR-12**	**RR-13**	**RR-14**	
Toluene	Toluene	Toluene	Toluene	Substance
$2.2 \cdot 10^{-5}$	$2.2 \cdot 10^{-5}$	$2.2 \cdot 10^{-5}$	$2.2 \cdot 10^{-5}$	Surface roughness length (m)
3.83	5.10	6.27	8.27	Wind speed (m/s)
10	10	10	10	Reference height for wind speed (m)

- Values for the surface thermal conductivity and diffusivity set to the limits in order to eliminate the heat contribution from the ground

Series		**Norman and Dowell**	
Spill		Instantaneous	
Spill duration (s)		0.001	
Pasquill stability class		F (stable)	
Reference height for wind speed (m)		10	
Atmospheric temperature (K)		293	
Atmospheric humidity (%)		35	
Solar radiation (W/m^2)		800	
Bund diameter (m)		0.915	
Surface temperature (K)		293	
Maximum simulation time (s)		7200	
Surface roughness factor		1	
Surface thermal conductivity (W/m.K)		0.1	
Surface thermal diffusivity (m^2/s)		$6 \cdot 10^{-7}$	
ND-A	**ND-B**	**ND-C**	
Ammonia	Acrylonitrile	n-Butane	Substance
44.8	24.3	19.6	Spill mass (kg)
239	293	272	Temperature of the spill (K)
5	1	1	Wind speed (m/s)
ND-D	**ND-E**	**ND-F**	
Ethylene Oxide	Propylene	Carbon Disulfide	Substance
28.7	20.1	41.55	Spill mass (kg)
283	225	293	Temperature of the spill (K)
1	1	1	Wind speed (m/s)

Series	**Okamoto et al.**		
Type of spill	Instantaneous		
Spill temperature (K)	273		
Air temperature (K)	273		
Bund surface area (m^2)	1.10^{-4}		
Bund radius (m)	$5.64.10^{-3}$		
Type of surface	Insulated		
	1	**2**	**3**
Spill mass (kg)	0.0997	0.0989	0.1319
Initial pool depth (m)	0.0015	0.0015	0.002
Spill composition (% mol/mol)			
n-Pentane	50	50	33.4
n-Hexane	50	0	33.3
n-Heptane	0	50	33.3

Series	**Habid et al.**		
Type of spill	Instantaneous		
Bund diameter (m)	0.74		
Type of surface	Insulated – User defined		
	1	**2**	**3**
Spill mass (kg)	5.14	5.14	5.14
Spill temperature (K)	302.85	302.85	302.85
Substance	Ethanol	Ethanol	Ethanol
Ambient temperature (K)	299.95	299.95	299.95
Wind speed at 10 m (m/s)	2.79	2.79	2.79
Solar radiation flux (W/m^2)	700	743	750
Cloud cover (%)	50	30	20
	4	**5**	**6**
Spill mass (kg)	5.27	5.27	5.27
Spill temperature (K)	299.55	299.55	299.55
Substance	Cyclohexane	Cyclohexane	Cyclohexane
Ambient temperature (K)	296.55	296.55	296.55
Wind speed at 10 m (m/s)	3.74	3.74	3.74
Solar radiation flux (W/m^2)	697	740	748
Cloud cover (%)	50	30	20

- Values for spill mass, atmospheric temperature and wind speed at 10 m height obtained by private communication with Habid
- Solar radiation flux estimated from cloud cover and solar elevation data as indicated in section 2.1

A.2 Pools on water

Series			**Bureau of Mines**
Spill			Instantaneous
Spill duration (s)			0.001
Pasquill stability class			F (stable)
Reference height for wind speed (m)			10
Wind speed at reference height (m/s)			0.1001
Atmospheric pressure (Pa)			101,325
Atmospheric temperature (K)			293.15
Solar radiation (W/m^2)			0
Surface temperature (K)			278.15
Type of surface			Deep water
Composition LNG1 (% v/v):			**Composition LNG2 (% v/v):**
91.2 Methane			94.74 Methane
6.2 Ethane			5.2 Ethane
0.1 Propane			0.04 Propane
1.2 Nitrogen			0.02 Butane
0.6 Oxygen			
0.7 Carbon dioxide			
BM 18-34	**BM 35-43**	**BM 44-60**	
LNG	Methane	Nitrogen	Substance
0.55	1	1	Mass spilled (kg)
111.66	111.66	77.34	Spill temperature (K)

- LNG was treated as a pseudo-component with the compositions provided by the authors.
- Deep water is chosen as surface as it gave the best fit to experimental data.
- Atmospheric temperature not provided by the authors, default value for indoors experiments was used.

Series	**Reid and Smith**
Pasquill stability class	F (stable)
Atmospheric pressure (Pa)	101,325
Atmospheric temperature (K)	293.15
Wind speed at reference height (m/s)	0.1001
Reference height for wind speed calculation (m)	10
Solar radiation (W/m^2)	0
Ice surface roughness factor	1
Ice thermal conductivity (W/m.K)	2.43
Ice thermal diffusivity (m^2/s)	$1.36 \cdot 10^{-6}$
Ice minimum thickness (m)	$5 \cdot 10^{-3}$

RS1	**RS2**	**RS3**	
Propane	Propane	Propane	Substance
Instantaneous	Continuous	Instantaneous	Spill
231	231	231	Spill temperature (K)
0.36	----	0.394	Spill mass (kg)
----	0.0788	----	Spill rate (kg/s)
0.001	5	0.001	Spill duration (s)
Ice-User Def.	Shallow water	Shallow water	Type of surface
272.65	295.15	295.15	Surface temperature (K)
0.1888	0.1559	0.1559	Bund diameter (m)
RS4	**RS5**	**RS6**	
Ethane	Ethylene	N-Butane	Substance
Instantaneous	Instantaneous	Instantaneous	Spill
185	169	273	Spill temperature (K)
0.217	0.2225	0.213	Spill mass (kg)
0.001	0.001	0.001	Spill duration (s)
Shallow water	Shallow water	Deep water	Type of surface
295.15	295.15	295.15	Surface temperature (K)
0.1559	0.1559	0.1559	Bund diameter (m)

- Atmospheric data not provided, from the scale of the experiment it is assumed to be indoors, and corresponding assumed values were used as indicated in Section 2.1.
- Ice roughness factor assumed as one, corresponding to a smooth surface.
- Ice thermal conductivity and thermal diffusivity taken from Reid and Smith[x].
- Reid and Smith[x] reported no ice formation for test run RS6, even for the small scale of the experiment. The mass vaporised follows a linear dependency on the time, unlike a square dependency evidenced in solid (ice) surfaces. Therefore, deep instead of shallow water was selected as the surface in order to model no ice formation.

Series			**Burro Series**	
Substance			Methane	
Spill			Continuous	
Spill temperature (K)			111.66	
Atmospheric pressure (Pa)			101,325	
Solar radiation (W/m^2)			500	
Reference height for wind speed calculation (m)			2	
Surface roughness length (m)			10^{-3}	
Type of surface			Deep water	
BU2	**BU3**	**BU4**	**BU5**	
83.79	85.91	85.20	79.57	Spill rate (kg/s)
173	167	175	190	Spill duration (s)
B	B	C	C	Pasquill stability class
311.27	307.75	309.05	314.27	Atmospheric temperature (K)
93,928.3	94,840.2	94,536.2	94,130.9	Atmospheric pressure (Pa)
7	5	2	6	Atmospheric humidity (%)
5.4	5.4	9	7.4	Wind speed at reference height (m/s)
311.15	307.40	308.90	314.06	Surface temperature (K)
BU6	**BU7**	**BU8**	**BU9**	
90.13	95.77	112.67	129.57	Spill rate (kg/s)
129	174	107	79	Spill duration (s)
C	C-D	E	D	Pasquill stability class
312.67	306.96	306.02	308.52	Atmospheric temperature (K)
93,523	94,030	94,131	94,030	Atmospheric pressure (Pa)
5	7	5	12	Atmospheric humidity (%)
9.1	8.4	1.8	5.7	Wind speed at reference height (m/s)
312.74	307.01	306.15	308.62	Surface temperature (K)

Series		**Dodge et al.**
Spill temperature (K)		298.15
Pasquill stability class		D (neutral)
Atmospheric temperature (K)		293.15
Atmospheric pressure (Pa)		101,325
Solar radiation (W/m^2)		500
Reference height for wind speed calculation (m)		10
Surface temperature (K)		293.15
Type of surface		Shallow water
Do IV. 1-4	**Do III. 1-3**	
n-Pentane	n-Pentane	Substance
Continuous	Instantaneous	Spill
---	25	Spill mass (kg)
0.79	---	Spill rate (kg/s)
60	n/a	Spill duration (s)
2.62	1.83	Wind speed at reference height (m/s)
Do II. 1-4	**Do I. 1-2**	
n-Octane	n-Octane	Substance
Continuous	Instantaneous	Spill
---	7.03	Spill mass (kg)
0.886	---	Spill rate (kg/s)
35	0.001	Spill duration (s)
0.1001	0.1001	Wind speed at reference height (m/s)

- Atmospheric stability class and atmospheric temperature not provided by the authors, outdoors default value were used.

Appendix B. Heat of evaporation equations

A literature review of the models available for evaporating pools showed the correlation most commonly found is MacKay and Matsugu[xxiii]. Opschoor[xxiv] model followed MacKay and Matsugu, incorporating a correction factor for high vapour pressure substances. PVAP in Phast 6.7 is a modification of this formula, made to obtain a better agreement to experimental data (Norman and Dowell[xvi] and Industrial Health and Engineering Associates) (Technica[xxxviii]). The following table shows the three equations for the heat of evaporation.

Opschoor[xxiv]	$Q_{evap} = 2 \cdot 10^{-3} \left[u_a (z = 10m)\right]^{0.78} r^{-0.11} \Delta H_{vap} \frac{M_c P_a}{RT_{pool}} \ln\left(\frac{P_a}{P_a - P^c{}_v (T_{pool})}\right)$
MacKay and Matsugu[xxiii]	$Q_{evap} = 0.004786\, \pi\, Sc^{-0.67} \left[u_a (z = 10\ m)\right]^{0.78} r^{1.89} \Delta H_{vap} \frac{M_c P_v{}^c}{RT_{pool}}$
PVAP in Phast 6.7	$Q_{evap} = 0.014\, \pi\, Sc^{-0.67} \left[u_a (z = 1\ m)\right]^{0.25} r^{1.89} \Delta H_{vap} \frac{M_c P_a}{RT_{pool}} \ln\left(\frac{P_a}{P_a - P_v^c (T_{pool})}\right)$

Table 9. Equations for the heat of evaporation that have been compared against experimental data in PVAP validation

About DNV

We are the independent expert in risk management and quality assurance. Driven by our purpose, to safeguard life, property and the environment, we empower our customers and their stakeholders with facts and reliable insights so that critical decisions can be made with confidence. As a trusted voice for many of the world's most successful organizations, we use our knowledge to advance safety and performance, set industry benchmarks, and inspire and invent solutions to tackle global transformations.

Digital Solutions

DNV is a world-leading provider of digital solutions and software applications with focus on the energy, maritime and healthcare markets. Our solutions are used worldwide to manage risk and performance for wind turbines, electric grids, pipelines, processing plants, offshore structures, ships, and more. Supported by our domain knowledge and Veracity assurance platform, we enable companies to digitize and manage business critical activities in a sustainable, cost-efficient, safe and secure way.

DNV | digital@dnv.com | dnv.com/digital

REFERENCES

[1] Prince, A.J. (1983) “Details and results of spill experiments of cryogenic liquids onto land and water” *Joint HSE and UKAEA, SRD Report, HSE/SRD/PD058/WP4.*

[2] Thyer, A.M. (1996). “A review of data available for estimating the rate of evaporation from chemical pools” *Health and Safety Laboratory.*

[3] Thyer, A.M. (2003) “A review of data on spreading and vaporisation of cryogenic spills” *Journal of Hazardous Materials* 99(1) 31-40.

[4] Luketa-Hanlin, A. (2006) “A review of large scale LNG spills: experiments and modelling” *Journal of Hazardous Materials* 132(2-3) 119-140.

[5] Hanna, S.R., D.G.Strimaitis, and J.C.Chang, (1991) “Hazard response modelling uncertainty (A quantitative method)”, Sigma Research Corp. report, Westford, MA for the API.

[6] Webber, D.M., Gant, S.E., Ivings, M.J. and Jager, S.J. (2009) “LNG source term models for hazard analysis: A review of the state-of-the-art and an approach to model assessment”, *The Fire Protection Research Foundation, Quincy MA., USA.*

[vii] Reid, R. C. and Wang, R. (1978). “The boiling rates of typical dike floors materials”. *Cryogenics* 18(7) 401-404.

[viii] Moorhouse, J. and Carpenter, R.J. (1986) “Factors affecting water evolution rates from liquefied gas spills”. *I. Chem.E North Western Branch Papers* No.1*.*

[ix] Burgess, D.S.; Biordi, J. and Murphy, J.N. (1972). “Hazards of spillage of LNG into water”. *U.S. Bureau of Mines.*

[x] Reid, R.C. and Smith, K.A. (1978) “Behaviour of LNG on water”. *Hydrocarbon Processing* 57(4) 117-121.

[xi] Koopman, R.P.; Cederwall, R.T.; Ermak, D.L.; Goldwire, H.C.; Hogan, W.J.; McClure, J.W.; McRae, T.G.; Morgan, D.L. and Shinn, J.H. (1980) “Analysis of Burro Series 40 m^3 LNG spill experiments” *Journal of Hazardous Materials* 6(1-2) 43-83.

[xii] Raj, P. P. K. and Reid, R. C., “Fate of liquid ammonia spilled onto water”, *Environmental Science & Technology* 12, pp. 1422-1425 (1978)

[xiii] Okamoto, K., Watanabe, N., Hagimoto, Y., Miwa, K., Ohtani, H. (2010)“Evaporation characteristics of multi-component liquids” *Journal of Loss Prevention in the Process Industries,* 23, pp 89-97.

[xiv] Belore, R. and McBean, E., (1986) “Modelling the spreading infiltration, and evaporation of chemical spills on grass and impermeable surfaces”. *Environment Canada, Environmental Protection Directorate*. Ottawa, Canada.

[xv] Kawamura, P.I. and MacKay, D. (1987). “The evaporation of volatile liquids”. *Journal of Hazardous Materials* 15(3) 343-364.

[xvi] Norman, E.C. and Dowell, H.A. (1980) “Using aqueous foams to lessen vaporisation from hazardous chemical spills”. *AIChE Loss Prevention* 13 pp. 27-34.

[xvii] Reijnhart, R. and Rose, R. (1980). “Vapour cloud dispersion and the evaporation of volatile liquids in atmospheric wind fields –II Wind tunnel experiments”. *Atmospheric Environment* 14(7) 759-762.

[xviii] Habid, A., Schalau, B., Acikalin, A., Steinbach, J. (2009) “Transient Calculation of the Boundary Layer Flow over Spills” Chem. Eng. Technol, 32, 2, pp 1-7.

[xix] Dodge, F.T.; Park, J.T.; Buckingham, J.C. and Magott, R.J. (1985). “Revision and experimental verification of the hazard assessment computer system models for spreading, movement, dissolution, and dissipation of insoluble chemicals spilled onto water”. *U.S. Department of Transportation.* Report CG-D-35-83.

[xx] Reijnhart, R.; Piepers, J. and Toneman, L.H. (1980). “Vapour cloud dispersion and the evaporation of volatile liquids in atmospheric wind fields –I Theoretical Model”. *Atmospheric Environment* 14(7) 751-758

[xxi] Van den Bosch (1996). “Pool evaporation”*. Methods for the calculation of physical effects due to releases of hazardous materials*. TNO.

[xxii] National Oceanic and Atmospheric Administration (NOAA), US Department of Commerce, http://www.esrl.noaa.gov/gmd/grad/solcalc/

[xxiii] MacKay, D., and R. S. Matsugu, (1973) “Evaporation rate of hydrocarbon spills on water and land”. *Can. J. Chem. Eng.,* 5 434–439.

[xxiv] Opschoor, G., “Methods for the calculation of the physical effects of the escape of dangerous material”, TNO Yellow Book, Ch. 5 (1979)

[xxv] Humbert-Basset, R., Montet, A. Dispersion dans l'atmosphere d'un nuage gazeux forme par epandage de G.N.L. sur le Sol, *Third International Conference on Liquefied National Gas*, Washington, DC, (September 1972)

[xxvi] Drake, E.M., Reid, R.C. How LNG boils on soils, *Hydro Proc* (May 1975) 191

[xxvii] Khajehnajafi, Shahryar and Pourdarvish, Reza (2011) “Correlations for Mass Transfer from a liquid Spill: Comparisons and Recommendations” *AIChE Process Safety Progress,* 30, 2, pp 178-184

[xxviii] Napier, D.H. and Roopchand, D.H., “An approach to hazard analysis of LNG spills”, J. Occupational Accidents 1, pp. 251-272 (1986)

[xxix] Burgess, D., Murphy, J., and Zabetakis, M. (1970). *Hazards of LNG spillage in marine transporation.* U.S. Bureau of Mines.

[xxx] Feldbauer, G.F., Heigl J.J., McQueen, W., Whip, R.H., May, W.G. (1972). *Spills of L.N.G. on water—Vaporization and downwind drift of combustible mixtures*. Esso Research and Engineering Company, Report: EE61E-72.

[xxxi] Webber, D.M., (1990) “A model of steady discharge into a vaporising pool”, *UKAEA* Report *SRD/HSE R493, Safety and Reliability Directorate, Warrington, UK.*

[xxxii] Webber, D.M., (1991) “Source terms”, *J. of Loss. Prev. in the Proc. Ind.* 1, 5-15.

[xxxiii] Webber, D.M., and Jones, S.J., (1987) “A model of spreading vaporising pools”, *Int. Conf. on Vapour Cloud Modelling, AIChE, Boston, Massacusetts, USA.*
[xxxiv] Webber, D.M. (1985) *Heat Conduction Under a Spreading Pool.* AEA Technology
[xxxv] Leonelli, P.; Stramigioli, C.; Spadoni, G. (1994). “The Modelling of Pool Vaporisation”. *J. Loss Prev. Process Ind.* 7(6) 443-450.
[xxxvi] Shaw, P. and Briscoe, F. (1980). “Spread and Evaporation of Liquid” *Prog. Energy Comb. Sci..* 6 127-140.
[xxxvii] Rohsenow, W.M.; Hartnett, J.P.; Cho, Y.I. (1998). *Handbook of Heat Transfer.* 3rd Edition, McGraw Hill, New York.
[xxxviii] DNV (1996) “Modification of Pool Evaporation Modelling for DNV Technica Product Programs”.